Journal of Statistical Physics manuscript No.
(will be inserted by the editor)

Gradient divergence of fluid-dynamic quantities in rarefied gases on smooth boundaries

Shigeru Takata · Satoshi Taguchi

July 16, 2017 (Received: date / Accepted: date)

Abstract The behavior of fluid-dynamic (or macroscopic) quantities of rarefied gases is studied, with a special interest in its non-analytic feature near boundaries. It is shown that their gradients normal to the boundary diverge even if the boundary is smooth, irrespective of the value of the (nonzero) Knudsen number. The boundary geometry determines the diverging rate. On a planar or concave boundary, the logarithmic divergence $\ln s$ should be observed, where s is the normal distance from the boundary. In other cases, the diverging rate is enhanced to be the inverse-power $s^{-1/n}$, where $n(\geq 2)$ is the degree of the dominant terms of the polynomial which locally represents the boundary. Some numerical demonstrations are given as well.

Keywords Boltzmann equation · kinetic theory · rarefied gas · singularity

1 Introduction

One of the characteristic features in gases at low pressure circumstances and/or in micro-scales, which we generically call rarefied gases, is the ballistic aspect in transport phenomena, which leads to the macroscopic behavior peculiar to those gases. In the present paper, we are going to clarify that the gradients of fluid dynamic quantities of rarefied gases, such as those of velocity and temperature in the normal direction, can blow up in approaching the boundary, even if the boundary and the distribution of physical quantities like temperature on it are smooth. Such phenomenon is never expected in the usual viscous fluid,

S. Takata
Department of Aeronautics and Astronautics, Kyoto University, Kyoto 615-8540, Japan
E-mail: takata.shigeru.4a@kyoto-u.ac.jp

S. Taguchi
Department of Mechanical and Intelligent Systems Engineering, The University of Electro-Communications, Chofu, Tokyo 182-8585, Japan (Present address: Department of Advanced Mathematical Sciences, Kyoto University, Kyoto 606-8501, Japan)

because the blow up of those gradients implies the infinite viscous force acting on the body and the infinite heat transfer to the body. The present paper largely extends our recent results in [13,14]; we are here going to establish a general view on the above issue, especially the diverging rate and its dependence on the boundary geometry, by a natural extension of the analyses in [13,14]. The key is the combination of two concepts: the occurrence of discontinuity at the microscopic level (i.e., at the level of the velocity distribution function) and the local geometry of the boundary. This combination makes our approach and main interest distinct from recent mathematical works on the related topics, e.g., [4,3,2]. The present work also gives an insight on the difference in structure between the S layer [6] and the Knudsen layer at their bottoms. The former is known to appear, in addition to the latter, around a convex body in the slip-flow regime, i.e., for small Knudsen numbers.

2 Prototype study of the formation of the gradient singularity

The (dimensionless) original Boltzmann equation can be written as [10]

$$\frac{\partial f}{\partial t} + \zeta_i \frac{\partial f}{\partial x_i} = J[f, f],$$

where $\boldsymbol{x}$ is the spatial coordinates, $\boldsymbol{\zeta}$ is the molecular velocity, f is the velocity distribution function of gas molecules, and J is the collision operator. Here we have included the Knudsen number in the definition of J. The linearized Boltzmann equation is obtained by putting $f = (1+\phi)E$ with $E = \pi^{-3/2}\exp(-\zeta_i^2)$ (the absolute Maxwellian at the reference equilibrium state at rest), and then by retaining only the first order terms of ϕ. The result is as follows:

$$\frac{\partial \phi}{\partial t} + \zeta_i \frac{\partial \phi}{\partial x_i} = \mathcal{L}[\phi],$$

where $\mathcal{L}[\phi] \equiv 2J[E, \phi E]/E$. For finite range or cutoff intermolecular potentials, $\mathcal{L}$ is known to take the form of [10]

$$\mathcal{L}[\phi] = -\nu(|\boldsymbol{\zeta}|)\phi + \mathcal{K}[\phi]. \tag{1}$$

We are going to study the solution for the steady linearized Boltzmann equation (possibly with a source)[1]over a smooth boundary:

$$\zeta_i \frac{\partial \phi}{\partial x_i} = \mathcal{L}[\phi] + S, \qquad \text{b.c. } \phi(\boldsymbol{x}_w, \boldsymbol{\zeta}) = \phi_w(\boldsymbol{x}_w, \boldsymbol{\zeta}),\ \boldsymbol{\zeta}\cdot\boldsymbol{n} > 0, \tag{2}$$

where S is a source term, ϕ_w represents the imposed data at the position $\boldsymbol{x}_w$ on the boundary, and $\boldsymbol{n}$ is the unit normal to the boundary, pointing to

[1] The source S arises in the equation, if we put $f = (1+\phi+g)E$ with g being a given function. Then, S is related to g as $S = -\zeta_i \frac{\partial g}{\partial x_i} + \mathcal{L}[g]$ and is usually analytic in both $\boldsymbol{x}$ and $\boldsymbol{\zeta}$. Such a formulation is common in treating, for instance, the Poiseuille and thermal creep (transpiration) flow problems. See, e.g., Refs [10,13].

the gas region. We suppose that the boundary is smooth enough for the unit normal $\boldsymbol{n}$ to be defined everywhere and that the boundary data ϕ_w is smooth. Throughout the paper, we use the dimensionless descriptions, unless otherwise stated.

The macroscopic quantities such as the density ρ, flow velocity u_i, temperature T, pressure p, stress tensor p_{ij}, and heat flow vector q_i are defined as the moments of f,

$$\rho = \int f d\boldsymbol{\zeta}, \quad \rho u_i = \int \zeta_i f d\boldsymbol{\zeta}, \quad p = \rho T = \frac{2}{3}\int (\zeta_i - u_i)^2 f d\boldsymbol{\zeta},$$
$$p_{ij} = 2\int (\zeta_i - u_i)(\zeta_j - u_j) f d\boldsymbol{\zeta}, \quad q_i = \int (\zeta_i - u_i)(\zeta_j - u_j)^2 f d\boldsymbol{\zeta},$$

and, after the linearization, their deviation from the reference equilibrium state at rest, namely $\omega \equiv \rho - 1$, u_i, $\tau \equiv T - 1$, $P \equiv p - 1$, $P_{ij} \equiv p_{ij} - \delta_{ij}$, and $Q_i \equiv q_i$, are expressed as the moments of ϕ: [10]

$$\omega = \int \phi E d\boldsymbol{\zeta}, \quad u_i = \int \zeta_i \phi E d\boldsymbol{\zeta}, \quad \tau = \frac{2}{3}\int (\zeta_i^2 - \frac{3}{2})\phi E d\boldsymbol{\zeta},$$
$$P_{ij} = 2\int \zeta_i \zeta_j \phi E d\boldsymbol{\zeta}, \quad Q_i = \int \zeta_i (\zeta_j^2 - \frac{5}{2})\phi E d\boldsymbol{\zeta}.$$

The central issue to be discussed is the possibility of the gradient of these quantities to diverge in the direction normal to the boundary, or, a little more generically, the possibility of

$$\frac{\partial}{\partial x_n}\langle \zeta_1^k \zeta_2^\ell \zeta_3^m \phi\rangle \to \pm\infty, \quad (k, \ell, m\text{: non-negative integers}),$$

when approaching the boundary, where $x_n = \boldsymbol{x}\cdot\boldsymbol{n}$ and $\langle\cdot\rangle = \int \cdot \exp(-|\boldsymbol{\zeta}|^2) d\boldsymbol{\zeta}$. We will discuss the diverging rate as well.

Our strategy is as follows. We first study the occurrence of singularities for the case

$$\zeta_i \frac{\partial \phi}{\partial x_i} = -\nu(|\boldsymbol{\zeta}|)\phi, \qquad \text{b.c. } \phi(\boldsymbol{x}_w, \boldsymbol{\zeta}) = \phi_w(\boldsymbol{x}_w, \boldsymbol{\zeta}),\ \boldsymbol{\zeta}\cdot\boldsymbol{n} > 0,$$

which we call a partial model. Then, we study the case with a source term, which we call a quasi-full model:

$$\zeta_i \frac{\partial \phi}{\partial x_i} = -\nu(|\boldsymbol{\zeta}|)\phi + S, \qquad \text{b.c. } \phi(\boldsymbol{x}_w, \boldsymbol{\zeta}) = \phi_w(\boldsymbol{x}_w, \boldsymbol{\zeta}),\ \boldsymbol{\zeta}\cdot\boldsymbol{n} > 0,$$

where S is no longer supposed to be analytic in $\boldsymbol{x}$. Rather its spatial derivative in the direction normal to the boundary may diverge with the same rate as the moments of ϕ of the partial model with the same boundary data. We will show that such a generalized source term S does not influence the structure of the singularities in the partial model. The property of S supposed above is motivated by that $\mathcal{K}[\phi]$ is also a moment of ϕ, even though it depends not only on $\boldsymbol{x}$ but also on $\boldsymbol{\zeta}$. Indeed, we have a strong numerical evidence [13] for

the linearized Boltzmann equation for hard-sphere molecules that $\mathcal{K}[\phi]$ shares the same property with the moments of ϕ in $\boldsymbol{x}$.[2] Hence, once the assumption on $\mathcal{K}[\phi]$ is admitted, the statements to be established for the quasi-full model apply to the original problem (2), because the property of S covers the key property of $\mathcal{K}[\phi]$ in $\boldsymbol{x}$. Our discussions to be developed also apply to the collisionless limit by setting $\nu \equiv 0$ in the partial model. In Sects. 2.1–2.3, we focus on a couple of simple boundary geometries. More general geometries will be considered in Sect. 3 on the basis of the results in Sects. 2.1–2.3.

2.1 Partial model

2.1.1 Over a planar boundary

Let us first consider the following slab problem:

$$\zeta_1 \frac{\partial \phi}{\partial x_1} + \zeta_2 \frac{\partial \phi}{\partial x_2} = -\nu\phi, \quad \text{b.c. } \phi(x_1 = \pm 1, x_2, \boldsymbol{\zeta}) = g_\pm(x_2, \boldsymbol{\zeta}),\ \zeta_1 \lessgtr 0, \tag{3}$$

where $g_\pm$ are given functions smooth in their arguments. We are going to solve (3) and study the half-range moments $\langle\cdot\rangle_+ = \int_{\zeta_1>0} \cdot \exp(-|\boldsymbol{\zeta}|^2) d\boldsymbol{\zeta}$ of ϕ. For later convenience, we introduce the notation

$$\tan\alpha = \frac{\zeta_2}{\zeta_1}, \quad X_1 = x_1 + 1, \quad \eta = \sqrt{\zeta_1^2 + \zeta_2^2}, \quad w = \zeta_3,$$

and express ϕ as a function of $(X_1, x_2, \alpha, \eta, w)$, in place of $(x_1, x_2, \zeta_1, \zeta_2, \zeta_3)$. Since the specific form of $g_\pm$ is not given, there is no reference position in x_2; thus, without loss of generality, we may consider ϕ only on the X_1-axis (or the x_1-axis). Then, the solution ϕ for $\zeta_1 > 0$ is written as

$$\phi(X_1, \boldsymbol{\zeta}) = g_-(y_w, \boldsymbol{\zeta}) \exp\left(-\frac{\nu X_1}{\eta \cos\alpha}\right), \quad y_w = -X_1 \tan\alpha,$$

where $\alpha \in (-\pi/2, \pi/2)$ and $0 < X_1 < 2$. Our concern is the behavior of the X_1-derivative of the following half-range moments:

$$\begin{aligned} I^{k,\ell,m} \equiv& \langle \eta^k \cos^\ell\alpha \sin^m\alpha\, \phi\rangle_+ \\ =& \int_{-\infty}^{\infty} dw \int_0^{\infty} d\eta \int_{-\pi/2}^{\pi/2} d\alpha\, \eta^{k+1} \cos^\ell\alpha \sin^m\alpha\, g_-(y_w, \boldsymbol{\zeta})\, e^{-\eta^2 - w^2 - \frac{\nu X_1}{\eta\cos\alpha}}, \end{aligned}$$

where k, ℓ, m (≥ 0) are integers. By direct calculation, we have

$$\begin{aligned} (I^{k,\ell,m})' &= -J^{k,\ell-1,m}[\eta \sin\alpha \partial_1 g_- + \nu g_-] \\ &= -J^{k+1,\ell-1,m+1}[\partial_1 g_-] - J^{k,\ell-1,m}[\nu g_-], \end{aligned} \tag{4}$$

$$J^{p,q,r}[h] = \int_{-\infty}^{\infty} dw \int_0^{\infty} d\eta \int_{-\pi/2}^{\pi/2} d\alpha\, \eta^p \cos^q\alpha \sin^r\alpha\, e^{-\eta^2 - w^2 - \frac{\nu X_1}{\eta\cos\alpha}} h(y_w, \boldsymbol{\zeta}),$$

[2] The assumption on $\mathcal{K}[\phi]$ becomes rigorous if we use the model kinetic equations like the Bhatnagar–Gross–Krook (BGK) model [1,15].

where $'$ represents the derivative with respect to X_1 (or x_1) and $\partial_1 g_-$ is the derivative of g_- with respect to its first argument. Remind that g_- is smooth. It is thus obvious that $J^{k,\ell-1,m}[\eta \sin\alpha g'_- + \nu g_-]$ is bounded for $\ell \geq 1$, because the integrand is bounded. Our task is, therefore, to examine its behavior for $\ell = 0$. By changing the integration variable α to $\mu = \cos\alpha$ ($0 < \arccos\mu < \pi$), we have

$$\begin{aligned} J^{k,-1,m}[h] =& I_+^{k,m}[h] + (-1)^m I_-^{k,m}[h], \\ I_\pm^{p,r}[h] =& \int_{-\infty}^{\infty} dw \int_0^{\infty} d\eta \int_0^1 \frac{d\mu}{\mu} \eta^p (1-\mu^2)^{\frac{r-1}{2}}\, e^{-\eta^2 - w^2 - \frac{\nu X_1}{\eta\mu}} \\ & \times h(\mp \frac{X_1\sqrt{1-\mu^2}}{\mu}, \pm\arccos\mu, \eta, w), \end{aligned}$$

which will be evaluated below.

Case A: $\nu >^{\exists} \delta > 0$ ***(damping case)*** Although the factor $(1-\mu^2)^{\frac{r-1}{2}}$ in the integrand of $I_\pm^{p,r}[h]$ diverges when $r = 0$ and $\mu \to 1$, its diverging rate is to the power of $-1/2$, which is integrable. Hence we here consider $I_\pm^{p,1}[1]$ for simplicity. Then,

$$\begin{aligned} I_\pm^{p,1}[1] &= \int_{-\infty}^{\infty} dw \int_0^{\infty} d\eta\, \eta^p e^{-\eta^2-w^2} \int_0^1 d\mu\, \frac{1}{\mu} e^{-\frac{\nu X_1}{\eta\mu}} \\ &= \int_{-\infty}^{\infty} dw \int_0^{\infty} d\eta\, \eta^p e^{-\eta^2-w^2} \mathrm{E}_1(\frac{\nu X_1}{\eta}) \\ &= \int_{-\infty}^{\infty} dw \int_0^{\infty} d\eta\, \eta^p e^{-\eta^2-w^2} [-\gamma - \ln(\frac{\nu X_1}{\eta}) + F_1(\frac{\nu X_1}{\eta})], \end{aligned}$$

where $\mathrm{E}_1(x) = \int_x^\infty t^{-1}e^{-t}dt$ and $F_1(x) = \gamma + \ln(x) + \mathrm{E}_1(x)$. Because $0 \leq F_1(x) \leq 2\sqrt{x}$,[3] the integrals of the first and last terms in the square brackets are bounded, and we are left with the factor $\ln X_1$ from the second term. We thus conclude the occurrence of the logarithmic divergence from both $J^{k+1,\ell-1,m+1}[\partial_1 g_-]$ and $J^{k,\ell-1,m}[\nu g_-]$ in (4) with $\ell = 0$ and $\nu \neq 0$.

Case B: $\nu \equiv 0$ ***(collisionless case)*** By the same reason as the previous case, we consider $I_\pm^{p,1}[h]$:

$$I_\pm^{p,1}[h] = \int_{-\infty}^{\infty} dw \int_0^{\infty} d\eta\, \eta^p e^{-\eta^2-w^2} \int_0^1 d\mu\, \frac{1}{\mu} h(\mp\frac{X_1}{\mu}\sqrt{1-\mu^2}, \pm\arccos\mu, \eta, w).$$

[3] By definition, $F_1(x) = \gamma + \ln(x) + \mathrm{E}_1(x) = \gamma - \int_x^1 t^{-1}dt + \int_x^\infty t^{-1}e^{-t}dt = \gamma - \int_x^1 t^{-1}(1-e^{-t})dt + \int_1^\infty t^{-1}e^{-t}dt$. It is easy to see that $x - F_1(x)$ is a monotonically increasing function and $F_1(0) = 0$, so that $x \geq F_1(x) \geq 0$ for $x > 0$. Since $2\sqrt{x} \geq x$ for $0 < x \leq 1$, the desired inequality holds in this interval. For $x > 1$, consider $g(x) \equiv 2\sqrt{x} - F_1(x)$. Then, g is a monotonically increasing function, because $g'(x) = x^{-1}(\sqrt{x} - 1 + e^{-x}) \geq 0$ for $x \geq 1$. Therefore, $g(x) \geq g(1) = 2 - \gamma - \int_1^\infty t^{-1}e^{-t} \geq 2 - \gamma - e^{-1} > 0$, which shows the desired inequality to hold for $x > 1$ as well.

In contrast to the previous case, here we retain h, because the last integral diverges if h is a constant. A proper assumption on h is required. Because of the collisionless case, νg_- vanishes and h is simply $\partial_1 g_-$, i.e., the variation of g_- along the boundary. We thus adopt the finite range, the decaying, or the periodic property in x_2 as a proper assumption on h (or $\partial_1 g_-$) to avoid an indefinite growth of the boundary data g_-.

Data with a finite range Suppose that there is a positive constant $a > 0$ such that $h(x, \boldsymbol{\zeta}) = 0$ for $|x| > a$. Then,

$$
\begin{aligned}
|I_{\pm}^{p,1}[h]| &= |\int_{-\infty}^{\infty} dw \int_0^{\infty} d\eta\, \eta^p e^{-\eta^2-w^2} \int_Z^1 d\mu\, \frac{1}{\mu} h(\mp \frac{X_1}{\mu}\sqrt{1-\mu^2}, \pm \arccos\mu, \eta, w)| \\
&\le \int_{-\infty}^{\infty} dw \int_0^{\infty} d\eta\, \eta^p h_{\max}(\eta, w) e^{-\eta^2-w^2} \int_Z^1 d\mu\, \mu^{-1},
\end{aligned}
$$

where

$$
h_{\max}(\eta, w) e^{-\eta^2-w^2} = \max_{|x|\le a,\, |\mu|\le 1} |h(x, \boldsymbol{\zeta})| e^{-|\boldsymbol{\zeta}|^2}, \quad Z = 1/\sqrt{1+(a/X_1)^2}.
$$

By direct calculation of the last integral, we have

$$
|I_{\pm}^{p,1}[h]| \le (\int_{-\infty}^{\infty} dw \int_0^{\infty} d\eta\, \eta^p e^{-\eta^2-w^2} h_{\max})[-\ln X_1 + \frac{1}{2}\ln(X_1^2 + a^2)],
$$

and the logarithmic singularity manifests itself. Although we have estimated $|I_{\pm}^{p,1}[h]|$ from above, the same singularity should occur as far as h does not vanish as $\mu \to Z$. We thus conclude the logarithmic singularity in this case.

Decaying data Suppose that there is a set of a positive constant $a > 0$ and a function g such that $|h(x, \boldsymbol{\zeta})| < g(\eta, w)/(|x| + a)$. Then,

$$
|I_{\pm}^{p,1}[h]| \le \int_{-\infty}^{\infty} dw \int_0^{\infty} d\eta\, \eta^p e^{-\eta^2-w^2} g \int_0^1 \frac{d\mu}{X_1\sqrt{1-\mu^2} + a\mu}.
$$

Direct calculation of the last integral yields

$$
\int_0^1 \frac{d\mu}{X_1\sqrt{1-\mu^2} + a\mu} = \int_0^{\pi/2} \frac{\cos\theta d\theta}{a\sin\theta + X_1\cos\theta} = \frac{(\pi/2)X_1 + a\ln(a/X_1)}{X_1^2 + a^2},
$$

showing the logarithmic singularity again. Although we give the upper estimate here, the same singularity should occur as far as h does not vanish as $\mu \to 0$. We thus conclude the logarithmic singularity in this case.

Periodic data Suppose that $h(x,\boldsymbol{\zeta}) = g(\eta, w)\exp(ikx)$ (k: a positive integer). Then,

$$\begin{aligned} I_{\pm}^{p,1}[h] &= \int_{-\infty}^{\infty} dw \int_0^{\infty} d\eta\, \eta^p g e^{-\eta^2-w^2} \int_0^1 \frac{d\mu}{\mu} e^{\mp ik\frac{X_1}{\mu}\sqrt{1-\mu^2}} \\ &= \int_{-\infty}^{\infty} dw \int_0^{\infty} d\eta\, \eta^p g e^{-\eta^2-w^2} (J_a \mp iJ_b), \end{aligned}$$

where

$$J_a = \int_0^1 \frac{d\mu}{\mu} \cos(k\frac{X_1}{\mu}\sqrt{1-\mu^2}), \quad J_b = \int_0^1 \frac{d\mu}{\mu} \sin(k\frac{X_1}{\mu}\sqrt{1-\mu^2}).$$

By direct calculation, we have

$$\begin{aligned} J_a =& -\frac{1}{2}\left[\mathrm{Ci}\left(-ikX_1\right) + \mathrm{Ci}\left(ikX_1\right)\right]\cosh\left(kX_1\right) - i\mathrm{Si}\left(ikX_1\right)\sinh\left(kX_1\right), \\ J_b =& \frac{\pi}{2}\exp(-kX_1), \end{aligned}$$

where Ci and Si are defined for all complex z as

$$\mathrm{Si}(z) = \int_0^z \frac{\sin(t)}{t} dt, \quad \mathrm{Ci}(z) = \gamma + \ln(z) + \int_0^z \frac{\cos(t)-1}{t} dt.$$

Obviously, J_b is regular. As to J_a, Si is entire, but Ci has a logarithmic singularity at the origin and has a branch cut along the negative real axis.[4] Therefore, the singularity in J_a is reduced to that in its first term:

$$-\frac{1}{2}\left[\mathrm{Ci}\left(-ikX_1\right) + \mathrm{Ci}\left(ikX_1\right)\right]\cosh\left(kX_1\right) = -\ln(kX_1)\cosh(kX_1),$$

namely J_a has a logarithmic singularity. Although here g (and h) has been assumed to be independent of μ, the same singularity should occur as far as h does not vanish as $\mu \to 0$. We thus conclude the logarithmic singularity in this case.

Summary In conclusion, the gradient of the moment $\partial I^{k,\ell,m}/\partial X_1$ normal to the boundary in (4) may diverge only when $\ell = 0$, irrespective of whether $\nu \equiv 0$ or not. The diverging rate in approaching the boundary is always logarithmic with respect to the normal distance from the boundary. Its occurrence is due to $J^{k,\ell-1,m}[\eta \sin\alpha \partial_1 g_- + \nu g_-]$ with $\ell = 0$ in (4). The former term in its argument represents the effect of spatial variation of the boundary data along the boundary, while the latter represents the "damping" effect embedded in the collision dynamics. Thus, the latter does not occur in the collisionless case $\nu \equiv 0$. The results obtained so far are striking in the sense that the singular behavior is observed even when the smooth data is imposed on the flat boundary.

[4] Here, the value on the negative real axis is taken as the limit from above.

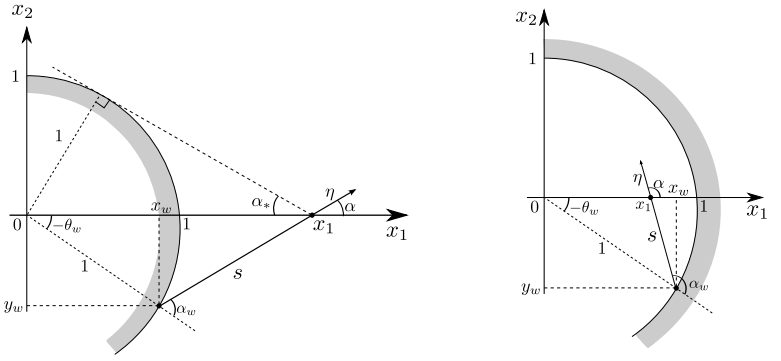

(a) Convex case (b) Concave case

Fig. 1 Boundary shape and notation. (a) Convex cylindrical boundary, (b) Concave cylindrical boundary.

2.1.2 Over a convex boundary

Consider the problem

$$\zeta_1 \frac{\partial \phi}{\partial x_1} + \zeta_2 \frac{\partial \phi}{\partial x_2} = -\nu\phi, \tag{5}$$

$$\text{b.c. } \phi = \begin{cases} g_+(\theta, \boldsymbol{\zeta}), & \boldsymbol{\zeta} \cdot \boldsymbol{n}(r=1,\theta) > 0, \\ g_-(\theta, \boldsymbol{\zeta}), & \boldsymbol{\zeta} \cdot \boldsymbol{n}(r=R,\theta) > 0, \end{cases}$$

where the spatial domain is $1 < r = \sqrt{x_1^2 + x_2^2} < R$ and $\tan\theta = x_2/x_1$ with $-\pi < \theta \leq \pi$. Since the form of $g_\pm$ is not specified, there is no reference direction. Hence, without loss of generality, we may restrict ourselves to study the behavior of the (partial) moments of ϕ when approaching the boundary along the positive x_1-axis.

Let us consider the solution of the problem for $x_2 = 0$ in the range $|\alpha| < \alpha_*$, where $\alpha_* \equiv \arcsin(1/x_1)$ and $\tan\alpha = \zeta_2/\zeta_1$ [or $\alpha = \arcsin(\zeta_2/\eta)$ with $\eta = \sqrt{\zeta_1^2 + \zeta_2^2}$] $(-\pi/2 < \alpha < \pi/2)$ [see Fig. 1(a)]. As before we denote ζ_3 by w and consider the moments of ϕ in the range $|\alpha| < \alpha_* (\leq \pi/2)$, because the VDF has a jump discontinuity, in general, across $\alpha = \pm\alpha_*$. Then, the solution in that range is written as[5]

$$\phi(x_1,0,\alpha,\eta,w) = g_+(\theta_w, \alpha_w, \eta, w) \exp(-\frac{\nu}{\eta} s),$$

$$s = (x_1^2 + 1 - 2x_1\cos\theta_w)^{1/2} = x_1\cos\alpha - (1 - x_1^2\sin^2\alpha)^{1/2},$$

$$x_w = \cos\theta_w = x_1 - s\cos\alpha = x_1\sin^2\alpha + (1 - x_1^2\sin^2\alpha)^{1/2}\cos\alpha,$$

[5] Here x_w is the x_1-coordinate of the intersection point of the molecular trajectory with the boundary. Hence x_w is one of the two solutions of $x_w^2 + (x_w - x_1)^2\tan^2\alpha = 1$ or $x_w^2 - 2x_w x_1\sin^2\alpha + x_1^2\sin^2\alpha - \cos^2\alpha = 0$. We adopt the larger of the solutions $x_w = x_1\sin^2\alpha \pm \cos\alpha(1 - x_1^2\sin^2\alpha)^{1/2}$, which is the one with a positive sign.

$$y_w = \sin\theta_w = -s\sin\alpha, \quad \alpha_w = \alpha - \theta_w.$$

The partial-range moments to be considered are written as

$$\begin{aligned} I_{\rm cv}^{k,\ell,m} &= \int_{-\infty}^{\infty} dw \int_0^{\infty} d\eta\, \eta \int_{-\alpha_*}^{\alpha_*} d\alpha\, \eta^k \cos^\ell\alpha\, \sin^m\alpha\, \phi\, e^{-\eta^2-w^2} \\ &= \int_{-\infty}^{\infty} dw \int_0^{\infty} d\eta \int_{-\alpha_*}^{\alpha_*} d\alpha\, \eta^{k+1} \cos^\ell\alpha\, \sin^m\alpha\, g_+(\theta_w,\alpha_w,\eta,w)\, e^{-\eta^2-w^2-\frac{\nu}{\eta}s}, \end{aligned}$$

where k, ℓ, m are non-negative integers. Remind that α_*, θ_w, α_w and s depend on x_1, so that their derivatives listed below occur when taking the derivative of $I_{\rm cv}^{k,\ell,m}$:

$$\begin{aligned} &s' = \cos\alpha + (x_1\sin^2\alpha)(1-x_1^2\sin^2\alpha)^{-1/2}, \quad y_w' = -s'\sin\alpha, \\ &x_w' = 1 - s'\cos\alpha = \sin^2\alpha\{1-(x_1\cos\alpha)(1-x_1^2\sin^2\alpha)^{-1/2}\}, \\ &\theta_w' = -\alpha_w' = -(1-x_1^2\sin^2\alpha)^{-1/2}\sin\alpha, \quad \alpha_*' = -\frac{1}{x_1(x_1^2-1)^{1/2}} = -\frac{\sin^2\alpha_*}{\cos\alpha_*}, \end{aligned}$$

where $'$ represents the partial derivative with respect to x_1. Under the preparation above, we have

$$\begin{aligned} \big(I_{\rm cv}^{k,\ell,m}\big)' &= \int_{-\infty}^{\infty} dw \int_0^{\infty} d\eta\, \alpha_*' \eta^{k+1} \cos^\ell\alpha_*\, \sin^m\alpha_* e^{-\eta^2-w^2-\frac{\nu}{\eta}s_*} \\ &\qquad \times [g_+(\theta_{w*},\alpha_{w*},\eta,w) + (-1)^m g_+(-\theta_{w*},-\alpha_{w*},\eta,w)] \\ &\quad + \int_{-\infty}^{\infty} dw \int_0^{\infty} d\eta \int_{-\alpha_*}^{\alpha_*} d\alpha\, \eta^{k+1} \cos^\ell\alpha\, \sin^m\alpha \\ &\qquad \times \theta_w' \,(\partial_1 g_+ - \partial_2 g_+)\, e^{-\eta^2-w^2-\frac{\nu}{\eta}s} \\ &\quad - \int_{-\infty}^{\infty} dw \int_0^{\infty} d\eta \int_{-\alpha_*}^{\alpha_*} d\alpha\, \nu\eta^k \cos^\ell\alpha\, \sin^m\alpha\, s' g_+\, e^{-\eta^2-w^2-\frac{\nu}{\eta}s} \\ &= -\int_{-\infty}^{\infty} dw \int_0^{\infty} d\eta\, \eta^{k+1} \cos^{\ell-1}\alpha_*\, \sin^{m+2}\alpha_* e^{-\eta^2-w^2-\frac{\nu}{\eta}s_*} \\ &\qquad \times [g_+(\theta_{w*},\alpha_{w*},\eta,w) + (-1)^m g_+(-\theta_{w*},-\alpha_{w*},\eta,w)] \\ &\quad - J_{\rm cv}^{k+1,\ell,m+1}[\partial_1 g_+ - \partial_2 g_+] - J_{\rm cv}^{k,\ell,m+2}[\nu x_1 g_+] \\ &\quad - \int_{-\infty}^{\infty} dw \int_0^{\infty} d\eta \int_{-\alpha_*}^{\alpha_*} d\alpha\, \nu\eta^k \cos^{\ell+1}\alpha\, \sin^m\alpha\, g_+\, e^{-\eta^2-w^2-\frac{\nu}{\eta}s} \\ &= -x_1^{-(m+\ell+1)}(x_1^2-1)^{\frac{\ell-1}{2}} I_{\rm cv}^{k+1,m}(x_1) \\ &\quad - J_{\rm cv}^{k,\ell,m+1}[\eta\partial_1 g_+ - \eta\partial_2 g_+ + x_1\nu\sin\alpha g_+] \\ &\quad - \int_{-\infty}^{\infty} dw \int_0^{\infty} d\eta \int_{-\alpha_*}^{\alpha_*} d\alpha\, \nu\eta^k \cos^{\ell+1}\alpha\, \sin^m\alpha\, g_+\, e^{-\eta^2-w^2-\frac{\nu}{\eta}s}, \end{aligned} \tag{6}$$

where

$$
\begin{aligned}
I^{p,q}_{\rm cv}(x_1) &= \int_{-\infty}^{\infty} dw \int_0^{\infty} d\eta\, \eta^p e^{-\eta^2-w^2-\frac{\nu}{\eta}s_*}[g_+(\theta_{w*},\alpha_{w*},\eta,w) \\
&\quad + (-1)^q g_+(-\theta_{w*},-\alpha_{w*},\eta,w)] \\
J^{p,q,r}_{\rm cv}[h] &= \int_{-\infty}^{\infty} dw \int_0^{\infty} d\eta \int_{-\alpha_*}^{\alpha_*} d\alpha\, \frac{\eta^p \cos^q\alpha\, \sin^r\alpha}{(1-x_1^2\sin^2\alpha)^{1/2}} e^{-\eta^2-w^2-\frac{\nu}{\eta}s} h,
\end{aligned}
$$

and the quantities with the subscript $*$ represent their values at $\alpha=\alpha_*$:

$$
\begin{aligned}
&x_1\sin\alpha_* = 1, \quad s_* = (x_1^2-1)^{1/2}, \quad \alpha_{w*} = \alpha_* - \theta_{w*}, \\
&x_{w*} = \cos\theta_{w*} = 1/x_1, \quad y_{w*} = \sin\theta_{w*} = -(x_1^2-1)^{1/2}/x_1.
\end{aligned}
$$

It is obvious that the last term of (6) remains finite for any $k,\ell,m(\geq 0)$ and that the first term of (6) remains finite for $\ell \geq 1$.

On the first term of (6) ***with*** $\ell = 0$ The first term with $\ell = 0$ is $-x_1^{-m-1}(x_1^2-1)^{-1/2} I^{k+1,m}_{\rm cv}(x_1)$, where the integral $I^{k+1,m}_{\rm cv}(x_1)$ remains finite. Thus, the first term diverge with the rate of $(x_1-1)^{-1/2}$ as $x_1 \searrow 1$, as far as $I^{k+1,m}_{\rm cv}(x_1)$ does not vanish in the same limit. It is indeed the case. Suppose that g_+ is a given constant, say $C>0$. Then, the integral is estimated from below as

$$
\begin{aligned}
|I^{k+1,m}_{\rm cv}(x_1)| &= C|1+(-1)^m| \int_{-\infty}^{\infty} dw \int_0^{\infty} d\eta\, \eta^{k+1}\, e^{-\eta^2-w^2-\frac{\nu}{\eta}s_*} \\
&= 2C|1+(-1)^m| \int_0^{\infty} d\zeta\, \zeta^{k+2} \int_0^{\pi/2} d\beta\, (\cos\beta)^{k+1}\, e^{-\zeta^2-\frac{\nu s_*}{\zeta\cos\beta}} \\
&\geq 2C|1+(-1)^m| \int_1^{2} d\zeta\, \zeta^{k+2}\, e^{-\zeta^2} \int_0^{\pi/2} d\beta\, (\cos\beta)^{k+1}\, e^{-\frac{2R\nu_{12}}{\cos\beta}} \\
&= 2C|1+(-1)^m| \int_1^{2} d\zeta\, \zeta^{k+2}\, e^{-\zeta^2} \int_1^{\infty} d\mu \frac{e^{-2R\nu_{12}\mu}}{\mu^{k+2}(\mu^2-1)^{1/2}} \\
&\geq 2^{-k-1}C|1+(-1)^m| [\int_1^2 d\zeta\, \zeta^{k+2} e^{-\zeta^2} \int_1^2 \frac{d\mu}{(\mu^2-1)^{1/2}}]\, e^{-4R\nu_{12}},
\end{aligned}
$$

where $\nu_{12} = \max_{1\leq\zeta\leq 2}\nu(\zeta)$. Therefore, the first term with $\ell=0$ diverges with the rate of $(x_1-1)^{-1/2}$ as $x_1 \searrow 1$ for the natural setting of the boundary data, at least for even m.

On the second term of (6) In order to examine the second term, let us consider $J_{\rm cv}^{k,\ell,m+1}[1]$. Then,

$$
\begin{aligned}
|J_{\rm cv}^{k,\ell,m+1}[1]| \le & \int_{-\infty}^{\infty} dw \int_0^{\infty} d\eta \int_{-\alpha_*}^{\alpha_*} d\alpha \frac{\eta^k \cos^\ell \alpha \, e^{-\eta^2 - w^2 - \frac{\nu}{\eta} s}}{(1 - x_1^2 \sin^2 \alpha)^{1/2}} \\
\le & 2 \int_{-\infty}^{\infty} dw e^{-w^2} \int_0^{\infty} d\eta \, e^{-\eta^2} \eta^k \int_0^{\alpha_*} d\alpha \frac{\cos^\ell \alpha}{(1 - x_1^2 \sin^2 \alpha)^{1/2}} \\
= & 2\sqrt{\pi} \int_0^{\infty} d\eta \, e^{-\eta^2} \eta^k \int_0^1 \frac{d\mu}{(1-\mu^2)^{1/2} x_1 [1 - (\mu/x_1)^2]^{(1-\ell)/2}} \\
\le & \begin{cases} 2\sqrt{\pi} (\int_0^{\infty} d\eta e^{-\eta^2} \eta^k) \frac{1}{x_1} K(\frac{1}{x_1}), & \ell = 0, \\ 2\sqrt{\pi} (\int_0^{\infty} d\eta e^{-\eta^2} \eta^k) \frac{1}{x_1} \int_0^1 \frac{d\mu}{(1-\mu^2)^{1/2}} & \ell \ge 1, \end{cases}
\end{aligned}
$$

where K is the complete elliptic integral of the first kind:

$$
K(a) \equiv \int_0^1 \frac{d\mu}{\sqrt{(1-\mu^2)(1-a^2\mu^2)}} \quad (0 < a^2 < 1).
$$

Because $K(a) \sim -(1/2)\ln(1-a^2)$ as $a \nearrow 1$, $|J_{\rm cv}^{k,\ell,m+1}[1]| \lesssim C \ln(1/(x_1 - 1))$ for $\ell = 0$ with a certain positive constant C. The diverging rate is, thus, at most logarithmic,which is much weaker than that of the first term with $\ell = 0$. For $\ell \ge 1$, neither the first nor the second term diverges.

Summary In conclusion, the gradient of the moment $\left(I_{\rm cv}^{k,\ell,m}\right)'$ in (6) can diverge again when $\ell = 0$, irrespective of whether $\nu \equiv 0$ or not. The dominant diverging rate is $1/\sqrt{x_1 - 1}$, which is by far stronger than the logarithmic one in the planar boundary case. This is due to the variation of the tangential direction to the boundary when the spatial point under consideration approaches the boundary along the x_1-axis. Therefore, it is a purely geometric effect [see the first term on the most right-hand side of (6)]. The result is again striking, because the singular behavior is induced even when the smooth data are imposed on the smooth convex boundary.

2.1.3 Over a concave boundary

Consider the problem

$$
\zeta_1 \frac{\partial \phi}{\partial x_1} + \zeta_2 \frac{\partial \phi}{\partial x_2} = -\nu \phi, \quad \text{b.c. } \phi = g_-(\theta, \boldsymbol{\zeta}), \ \boldsymbol{\zeta} \cdot \boldsymbol{n}(r = 1, \theta) > 0, \tag{7}
$$

where the spatial domain is $x_1^2 + x_2^2 < 1$ and $\tan\theta = x_2/x_1$ with $-\pi < \theta \le \pi$. By the same reason as before, without loss of generality, we may restrict ourselves to study the behavior of moments of ϕ when approaching the boundary along the x_1-axis [see Fig. 1(b)].

Let us introduce α and η by $\zeta_1 = \eta\cos\alpha$ and $\zeta_2 = \eta\sin\alpha$, denote ζ_3 by w as before, and consider the moments of ϕ for the entire range of α. Then, the solution is written as

$$\begin{aligned}\phi(x_1,0,&\alpha,\eta,w) = g_-(\theta_w,\alpha_w,\eta,w)\exp(-\frac{\nu}{\eta}s), \qquad -\pi<\alpha<\pi, \qquad (8)\\ &s = x_1\cos\alpha + (1-x_1^2\sin^2\alpha)^{1/2},\\ &x_w = \cos\theta_w = x_1 - s\cos\alpha = x_1\sin^2\alpha - (1-x_1^2\sin^2\alpha)^{1/2}\cos\alpha,\\ &y_w = \sin\theta_w = -s\sin\alpha, \quad \alpha_w = \alpha - \theta_w,\end{aligned}$$

and the moments to be considered at the position $(x_1, 0)$ are written as

$$\begin{aligned}I_{\rm cc}^{k,\ell,m} \equiv&\langle\eta^k\,\cos^\ell\alpha\,\sin^m\alpha\,\phi\rangle\\ =&\int_{-\infty}^{\infty}dw\int_0^{\infty}d\eta\,\eta\int_{-\pi}^{\pi}d\alpha\,\eta^k\cos^\ell\alpha\,\sin^m\alpha\,\phi\,e^{-\eta^2-w^2}\\ =&\int_{-\infty}^{\infty}dw\int_0^{\infty}d\eta\int_{-\pi}^{\pi}d\alpha\,\eta^{k+1}\cos^\ell\alpha\,\sin^m\alpha\,g_-(\theta_w,\alpha_w,\eta,w)\,e^{-\eta^2-w^2-\frac{\nu}{\eta}s},\end{aligned}$$

where k, ℓ, m are non-negative integers. Because θ_w, α_w and s depend on x_1, their derivatives listed below occur when taking the derivative of $I_{\rm cv}^{k,\ell,m}$:

$$\begin{aligned}&s' = \cos\alpha - (x_1\sin^2\alpha)(1-x_1^2\sin^2\alpha)^{-1/2},\\ &x_w' = 1 - s'\cos\alpha = \sin^2\alpha\{1 + (x_1\cos\alpha)(1-x_1^2\sin^2\alpha)^{-1/2}\},\\ &\theta_w' = -\alpha_w' = (1-x_1^2\sin^2\alpha)^{-1/2}\sin\alpha,\end{aligned}$$

where $'$ represents the partial derivative with respect to x_1. Under the preparation above, we have

$$\begin{aligned}\left(I_{\rm cc}^{k,\ell,m}\right)' =&\int_{-\infty}^{\infty}dw\int_0^{\infty}d\eta\int_{-\pi}^{\pi}d\alpha\,\eta^{k+1}\cos^\ell\alpha\,\sin^m\alpha\\ &\times(\partial_1 g_- - \partial_2 g_-)\theta_w'\,e^{-\eta^2-w^2-\frac{\nu}{\eta}s}\\ &-\int_{-\infty}^{\infty}dw\int_0^{\infty}d\eta\int_{-\pi}^{\pi}d\alpha\,\nu\eta^k\cos^\ell\alpha\,\sin^m\alpha\,g_-s'\,e^{-\eta^2-w^2-\frac{\nu}{\eta}s}\\ =&J_{\rm cc}^{k,\ell,m+1}[\eta\partial_1 g_- - \eta\partial_2 g_- + x_1\nu\sin\alpha g_-]\\ &-\int_{-\infty}^{\infty}dw\int_0^{\infty}d\eta\int_{-\pi}^{\pi}d\alpha\,\nu\eta^k\cos^{\ell+1}\alpha\,\sin^m\alpha\,g_-\,e^{-\eta^2-w^2-\frac{\nu}{\eta}s}, \qquad (9)\end{aligned}$$

where

$$J_{\rm cc}^{p,q,r}[h] = \int_{-\infty}^{\infty}dw\int_0^{\infty}d\eta\int_{-\pi}^{\pi}d\alpha\,\frac{\eta^p\cos^q\alpha\,\sin^r\alpha}{(1-x_1^2\sin^2\alpha)^{1/2}}e^{-\eta^2-w^2-\frac{\nu}{\eta}s}h.$$

It is obvious that the last term of (9) remains finite for any $k, \ell, m(\geq 0)$.

Estimate of the first term of (9) The estimate is almost parallel to that of the second term of (6) in Sect. 2.1.2. Because the integrand diverges when $\sin\alpha \to \pm 1$ when $x_1 = 1$, it is required to split the range of integration with respect to α into $(-\pi, -\pi/2)$, $(-\pi/2, \pi/2)$ and $(\pi/2, \pi)$. The value of s largely differs between the ranges $\alpha \in (-\pi/2, \pi/2)$ and $\alpha \in (-\pi, -\pi/2) \cup (\pi/2, \pi)$, especially when x_1 is close to unity. Thus, the contributions from the two ranges are not expected to cancel out each other. Keeping this in mind, we consider only the range $\alpha \in (-\pi, -\pi/2) \cup (\pi/2, \pi)$, especially its half range because only the even part of the integrand contributes. Our task is thus reduced to study the following integral:

$$\tilde{J}_{\rm cc} = \int_{-\infty}^{\infty} dw \int_0^{\infty} d\eta \int_{\pi/2}^{\pi} d\alpha\, \eta^k \frac{\cos^\ell\alpha\, \sin^{m+1}\alpha}{(1 - x_1^2 \sin^2\alpha)^{1/2}}\, e^{-\eta^2 - w^2 - \frac{\nu}{\eta} s},$$

and we have its upper estimate as

$$\begin{aligned} |\tilde{J}_{\rm cc}| &\le \int_{-\infty}^{\infty} dw \int_0^{\infty} d\eta \int_{\pi/2}^{\pi} d\alpha\, \eta^k \frac{|\cos^\ell\alpha|}{\sqrt{1 - x_1^2 \sin^2\alpha}}\, e^{-\eta^2 - w^2} \\ &= \sqrt{\pi} \int_0^{\infty} d\eta e^{-\eta^2} \eta^k \int_0^1 \frac{d\mu}{(1-\mu^2)^{(1-\ell)/2}(1 - x_1^2\mu^2)^{1/2}} \\ &\le \begin{cases} \sqrt{\pi}(\int_0^{\infty} d\eta e^{-\eta^2}\eta^k) K(x_1), & \ell = 0, \\ \sqrt{\pi}(\int_0^{\infty} d\eta e^{-\eta^2}\eta^k) \int_0^1 \frac{d\mu}{(1 - x_1^2\mu^2)^{1/2}}, & \ell \ge 1. \end{cases} \end{aligned} \tag{10}$$

On one hand, $|\tilde{J}_{\rm cc}| \lesssim C \ln(1 - x_1)$ for $\ell = 0$, because $K(a) \sim -(1/2)\ln(1 - a^2)$ as $a \nearrow 1$. On the other hand, because $(0 <) x_1 < 1$,

$$\int_0^1 \frac{d\mu}{(1 - x_1^2\mu^2)^{1/2}} \le \int_0^1 \frac{d\mu}{(1 - x_1\mu)^{1/2}} = \frac{2}{x_1}[1 - (1 - x_1)^{1/2}],$$

and thus $|\tilde{J}_{\rm cc}|$ remains finite for $\ell \ge 1$.

The lower estimate for the case $\ell = 0$ is obtained as follows:

$$\begin{aligned} |\tilde{J}_{\rm cc}| &= \int_{-\infty}^{\infty} dw \int_0^{\infty} d\eta \int_{\pi/2}^{\pi} d\alpha \frac{\eta^k \sin^{m+1}\alpha}{(1 - x_1^2\sin^2\alpha)^{1/2}} e^{-\eta^2 - w^2 - \frac{\nu}{\eta} s} \\ &= 2\int_0^{\infty} d\zeta \int_0^{\pi/2} d\beta \int_{\pi/2}^{\pi} d\alpha \frac{\zeta^{k+1}\cos^k\beta \sin^{m+1}\alpha}{(1 - x_1^2\sin^2\alpha)^{1/2}} e^{-\zeta^2 - \frac{\nu s}{\zeta\cos\beta}} \\ &\ge 2(\int_1^2 d\zeta \zeta^{k+1} e^{-\zeta^2})(\int_0^{\pi/2} d\beta e^{-\frac{2\nu_{12}}{\cos\beta}} \cos^k\beta) \int_0^1 \frac{\mu^{m+1} d\mu}{(1-\mu^2)^{1/2}(1 - x_1^2\mu^2)^{1/2}} \\ &\ge 2^{-m}(\int_1^2 d\zeta \zeta^{k+1} e^{-\zeta^2})(\int_0^{\pi/2} d\beta e^{-\frac{2\nu_{12}}{\cos\beta}} \cos^k\beta) \int_{1/2}^1 \frac{d\mu}{\sqrt{(1-\mu^2)(1 - x_1^2\mu^2)}} \\ &= 2^{-m}(\int_1^2 d\zeta \zeta^{k+1} e^{-\zeta^2})(\int_0^{\pi/2} d\beta e^{-\frac{2\nu_{12}}{\cos\beta}} \cos^k\beta)[K(x_1) - F(\frac{1}{2}, x_1)], \end{aligned}$$

where F is the incomplete elliptic integral of the first kind

$$F(x,a) \equiv \int_0^x \frac{dt}{\sqrt{(1-t^2)(1-a^2t^2)}}, \qquad (0 < a^2 < 1),$$

and behaves regularly in a as $a \nearrow 1$. Thus, K is dominant and $|\tilde{J}_{\rm cc}|$ is estimated to diverge with the common rate from both side.

Summary In conclusion, the gradient of the moment $\left(I_{\rm cc}^{k,\ell,m}\right)'$ in (9) may diverge again only when $\ell = 0$, irrespective of whether $\nu \equiv 0$ or not. The diverging rate is logarithmic, which is weaker than the convex case and is the same as the planar case. The result is again striking, because the singular behavior is mostly induced even when smooth data are imposed on the smooth concave boundary.

2.2 Quasi-full model

2.2.1 Over a planar boundary

We now consider the slab problem for the quasi-full model

$$\zeta_1 \frac{\partial \phi}{\partial x_1} + \zeta_2 \frac{\partial \phi}{\partial x_2} = -\nu\phi + S, \quad \text{b.c. } \phi(x_1 = \pm 1, x_2, \boldsymbol{\zeta}) = g_\pm(x_2, \boldsymbol{\zeta}),\ \zeta_1 \lessgtr 0, \tag{11}$$

which is obtained by adding the source S to the equation of problem (3). Here, we suppose that $S(x_1, x_2, \boldsymbol{\zeta})$ behaves in the same way as the moments of ϕ for the partial model and thus its derivative with respect to x_1 may diverge logarithmically in approaching the boundary. We use the same notation as in Sect. 2.1.1.

The solution ϕ for $\zeta_1 > 0$ is written as

$$\phi(X_1, 0, \boldsymbol{\zeta}) = g_-(y_w, \boldsymbol{\zeta}) e^{-\frac{\nu X_1}{\eta \cos\alpha}} + \int_0^{\frac{X_1}{\cos\alpha}} \frac{1}{\eta} e^{\frac{\nu}{\eta}(t - \frac{X_1}{\cos\alpha})} S(\tilde{x}, \tilde{y}, \boldsymbol{\zeta}) dt,$$

where $\alpha \in (-\pi/2, \pi/2)$, $y_w = -X_1 \tan\alpha$, $\tilde{x} = t\cos\alpha$, and $\tilde{y} = y_w + t\sin\alpha$. The half-range moments at the position $(X_1, 0)$ are then given by substitution as

$$\begin{aligned} I^{k,\ell,m} =& \langle \eta^k \cos^\ell\alpha \sin^m\alpha\, \phi \rangle_+ \\ =& \int_{-\infty}^{\infty} dw \int_0^{\infty} d\eta \int_{-\pi/2}^{\pi/2} d\alpha\, \eta^{k+1} \cos^\ell\alpha \sin^m\alpha\, g_-(y_w, \boldsymbol{\zeta})\, e^{-\eta^2 - w^2 - \frac{\nu X_1}{\eta\cos\alpha}} \\ &+ \int_{-\infty}^{\infty} dw \int_0^{\infty} d\eta \int_{-\pi/2}^{\pi/2} d\alpha\, \eta^k \cos^\ell\alpha \sin^m\alpha\, e^{-\eta^2 - w^2} \\ &\qquad \times \int_0^{\frac{X_1}{\cos\alpha}} e^{\frac{\nu}{\eta}(t - \frac{X_1}{\cos\alpha})} S(\tilde{x}, \tilde{y}, \boldsymbol{\zeta}) dt, \end{aligned}$$

where k, ℓ, m (≥ 0) are integers. The difference from the partial model case is the second term on the right-hand side. Then, by direct calculation, we have

$$\begin{aligned}
\left(I^{k,\ell,m}\right)' =& - J^{k,\ell-1,m}[\eta \sin\alpha \partial_1 g_- + \nu g_-] \\
&+ \int_{-\infty}^{\infty} dw \int_0^{\infty} d\eta \int_{-\pi/2}^{\pi/2} d\alpha\, \eta^k \cos^{\ell-1}\alpha\, \sin^m \alpha\, e^{-\eta^2-w^2} S(X_1, 0, \boldsymbol{\zeta}) \\
&- \int_{-\infty}^{\infty} dw \int_0^{\infty} d\eta \int_{-\pi/2}^{\pi/2} d\alpha\, \eta^{k-1}\nu \cos^{\ell-1}\alpha\, \sin^m \alpha\, e^{-\eta^2-w^2} \\
&\qquad \times \int_0^{\frac{X_1}{\cos\alpha}} e^{\frac{\nu}{\eta}(t-\frac{X_1}{\cos\alpha})} S(\tilde{x}, \tilde{y}, \boldsymbol{\zeta}) dt \\
&- \int_{-\infty}^{\infty} dw \int_0^{\infty} d\eta \int_{-\pi/2}^{\pi/2} d\alpha\, \eta^{k} \cos^{\ell-1}\alpha\, \sin^{m+1} \alpha\, e^{-\eta^2-w^2} \\
&\qquad \times \int_0^{\frac{X_1}{\cos\alpha}} e^{\frac{\nu}{\eta}(t-\frac{X_1}{\cos\alpha})} \partial_2 S(\tilde{x}, \tilde{y}, \boldsymbol{\zeta}) dt, \qquad (12)
\end{aligned}$$

where $\partial_2 S$ and $\partial_1 S$ that will appear soon later denote the derivatives of S with respect to its second and first arguments, respectively. Since

$$\int_0^{\frac{X_1}{\cos\alpha}} e^{\frac{\nu}{\eta}(t-\frac{X_1}{\cos\alpha})} dt = \frac{\eta}{\nu}(1 - e^{-\frac{\nu X_1}{\eta\cos\alpha}}),$$

$S(X_1, 0, \boldsymbol{\zeta})$ is rewritten as

$$S(X_1, 0, \boldsymbol{\zeta}) = e^{-\frac{\nu X_1}{\eta\cos\alpha}} S(X_1, 0, \boldsymbol{\zeta}) + \frac{\nu}{\eta} \int_0^{\frac{X_1}{\cos\alpha}} e^{\frac{\nu}{\eta}(t-\frac{X_1}{\cos\alpha})} S(X_1, 0, \boldsymbol{\zeta}) dt.$$

Substituting this into the second line of (12), we further transform (12) as follows:

$$\begin{aligned}
\left(I^{k,\ell,m}\right)' =& - J^{k,\ell-1,m}[\eta \sin\alpha \partial_1 g_- + \nu g_-] \\
&+ \int_{-\infty}^{\infty} dw \int_0^{\infty} d\eta \int_{-\pi/2}^{\pi/2} d\alpha\, \eta^k \cos^{\ell-1}\alpha\, \sin^m \alpha \\
&\qquad \times e^{-\eta^2-w^2-\frac{\nu X_1}{\eta\cos\alpha}} S(X_1, 0, \boldsymbol{\zeta}) \\
&- \int_{-\infty}^{\infty} dw \int_0^{\infty} d\eta \int_{-\pi/2}^{\pi/2} d\alpha\, \eta^{k-1}\nu \cos^{\ell-1}\alpha\, \sin^m \alpha\, e^{-\eta^2-w^2} \\
&\qquad \times \int_0^{\frac{X_1}{\cos\alpha}} e^{\frac{\nu}{\eta}(t-\frac{X_1}{\cos\alpha})} [S(\tilde{x}, \tilde{y}, \boldsymbol{\zeta}) - S(X_1, 0, \boldsymbol{\zeta})] dt \\
&- \int_{-\infty}^{\infty} dw \int_0^{\infty} d\eta \int_{-\pi/2}^{\pi/2} d\alpha\, \eta^{k} \cos^{\ell-1}\alpha\, \sin^{m+1} \alpha\, e^{-\eta^2-w^2} \\
&\qquad \times \int_0^{\frac{X_1}{\cos\alpha}} e^{\frac{\nu}{\eta}(t-\frac{X_1}{\cos\alpha})} \partial_2 S dt
\end{aligned}$$

$$
\begin{aligned}
&= - J^{k,\ell-1,m}[\eta \sin\alpha \partial_1 g_- + \nu g_- - S(X_1,0,\boldsymbol{\zeta})] \\
&\quad + \int_{-\infty}^{\infty} dw \int_0^{\infty} d\eta \int_{-\pi/2}^{\pi/2} d\alpha\, \eta^k \cos^{\ell-1}\alpha\, \sin^m \alpha\, e^{-\eta^2-w^2} \\
&\qquad \times \{e^{-\frac{\nu X_1}{\eta\cos\alpha}}[S(0,y_w,\boldsymbol{\zeta}) - S(X_1,0,\boldsymbol{\zeta})] + \int_0^{\frac{X_1}{\cos\alpha}} e^{\frac{\nu}{\eta}(t-\frac{X_1}{\cos\alpha})} \partial_t S dt\} \\
&\quad - \int_{-\infty}^{\infty} dw \int_0^{\infty} d\eta \int_{-\pi/2}^{\pi/2} d\alpha\, \eta^k \cos^{\ell-1}\alpha\, \sin^{m+1}\alpha\, e^{-\eta^2-w^2} \\
&\qquad \times \int_0^{\frac{X_1}{\cos\alpha}} e^{\frac{\nu}{\eta}(t-\frac{X_1}{\cos\alpha})} \partial_2 S dt \\
&= - J^{k,\ell-1,m}[\eta \sin\alpha \partial_1 g_- + \nu g_- - S(0,y_w,\boldsymbol{\zeta})] \\
&\quad + \int_{-\infty}^{\infty} dw \int_0^{\infty} d\eta \int_{-\pi/2}^{\pi/2} d\alpha\, \eta^k \cos^{\ell}\alpha\, \sin^{m}\alpha\, e^{-\eta^2-w^2} \\
&\qquad \times \int_0^{\frac{X_1}{\cos\alpha}} e^{\frac{\nu}{\eta}(t-\frac{X_1}{\cos\alpha})} \partial_1 S dt. \qquad (13)
\end{aligned}
$$

In the above transformation, we have used the integration by part for the second equality and the relation $\partial_t S(\tilde{x},\tilde{y},\boldsymbol{\zeta}) = \cos\alpha \partial_1 S(\tilde{x},\tilde{y},\boldsymbol{\zeta}) + \sin\alpha \partial_2 S(\tilde{x},\tilde{y},\boldsymbol{\zeta})$ for the last equality. Because the first term on the most right-hand side is the same integration as that occurring in the partial model, the remaining task is to study the contribution from the second term with keeping in mind that $\partial_1 S(\tilde{x},\cdot,\cdot)$ may behave like $\ln\tilde{x}$ for $0 < \tilde{x} < X_1 \ll 1$, where $\tilde{x} = t\cos\alpha$. We thus finally reduce the problem to study the behavior of

$$
J \equiv \int_{-\infty}^{\infty} dw \int_0^{\infty} d\eta \int_{-\pi/2}^{\pi/2} d\alpha\, \eta^k \cos^{\ell}\alpha\, \sin^m \alpha\, e^{-\eta^2-w^2} \int_0^{\frac{X_1}{\cos\alpha}} e^{\frac{\nu}{\eta}(t-\frac{X_1}{\cos\alpha})} \ln(t\cos\alpha) dt.
$$

Since $X_1 \ll 1$, we have

$$
\begin{aligned}
|J| &\le - \int_{-\infty}^{\infty} dw \int_0^{\infty} d\eta \int_{-\pi/2}^{\pi/2} d\alpha\, \eta^k e^{-\eta^2-w^2} \int_0^{\frac{X_1}{\cos\alpha}} e^{\frac{\nu}{\eta}(t-\frac{X_1}{\cos\alpha})} \ln(t\cos\alpha) dt \\
&= - \int_{-\infty}^{\infty} dw \int_0^{\infty} d\eta \int_{-\pi/2}^{\pi/2} d\alpha\, \eta^k e^{-\eta^2-w^2} \\
&\qquad \times \frac{\eta}{\nu}\{[e^{-\frac{\nu X_1}{\eta\cos\alpha}}(e^{\frac{\nu}{\eta}t}-1)\ln(t\cos\alpha)]_0^{\frac{X_1}{\cos\alpha}} - \int_0^{\frac{X_1}{\cos\alpha}} t^{-1} e^{-\frac{\nu X_1}{\eta\cos\alpha}}(e^{\frac{\nu}{\eta}t}-1) dt\} \\
&= - \int_{-\infty}^{\infty} dw \int_0^{\infty} d\eta \int_{-\pi/2}^{\pi/2} d\alpha\, \nu^{-1}\eta^{k+1} e^{-\eta^2-w^2} \\
&\qquad \times [(1-e^{-\frac{\nu X_1}{\eta\cos\alpha}})\ln X_1 - e^{-\frac{\nu X_1}{\eta\cos\alpha}} G(\frac{\nu X_1}{\eta\cos\alpha})],
\end{aligned}
$$

where $G(x) = \int_0^x t^{-1}(e^t - 1)dt$. Because $0 \le G(x) \le 2\sqrt{x}e^x$,[6]

$$
\begin{aligned}
|J| \le & -\ln X_1 \int_{-\infty}^{\infty} dw \int_0^{\infty} d\eta \int_{-\pi/2}^{\pi/2} d\alpha\, \nu^{-1}\eta^{k+1} e^{-\eta^2-w^2}(1 - e^{-\frac{\nu X_1}{\eta\cos\alpha}}) \\
& + 2X_1^{1/2} \int_{-\infty}^{\infty} dw \int_0^{\infty} d\eta \nu^{-1/2}\eta^{k+1/2} e^{-\eta^2-w^2} \int_{-\pi/2}^{\pi/2} d\alpha\, (\cos\alpha)^{-1/2} \\
\le & -2\ln X_1 \int_0^{\infty} d\zeta\, \nu^{-1}\zeta^{k+2} e^{-\zeta^2} \int_{-\pi/2}^{\pi/2} d\beta\, (\cos\beta)^{k+1} \int_0^1 d\mu\, \frac{(1 - e^{-\frac{\nu X_1}{\zeta\mu\cos\beta}})}{\sqrt{1-\mu^2}} \\
& + 8\sqrt{2}X_1^{1/2} \int_{-\infty}^{\infty} dw \int_0^{\infty} d\eta \nu^{-1/2}\eta^{k+1/2} e^{-\eta^2-w^2} \int_0^{1/2} \frac{d\mu}{\sqrt{\mu}}.
\end{aligned}
$$

For $\epsilon \ll 1$ and $a > 0$,

$$
\begin{aligned}
\int_0^1 d\mu\, \frac{1 - e^{-\frac{a}{\mu}}}{\sqrt{1-\mu^2}} &= \int_0^{\epsilon} d\mu\, \frac{1 - e^{-\frac{a}{\mu}}}{\sqrt{1-\mu^2}} + \int_{\epsilon}^1 d\mu\, \frac{1 - e^{-\frac{a}{\mu}}}{\sqrt{1-\mu^2}} \\
&\le \int_0^{\epsilon} d\mu\, \frac{1}{\sqrt{1-\epsilon^2}} + \int_{\epsilon}^1 d\mu\, \frac{1 - e^{-\frac{a}{\epsilon}}}{\sqrt{1-\mu}} \\
&= \frac{\epsilon}{\sqrt{1-\epsilon^2}} + 2\sqrt{1-\epsilon}(1 - e^{-\frac{a}{\epsilon}}) \le 2(\epsilon + 1 - e^{-\frac{a}{\epsilon}}).
\end{aligned}
$$

Using the above, we have

$$
\begin{aligned}
|J| \le & -4\ln X_1 \int_0^{\infty} d\zeta\, \nu^{-1}\zeta^{k+2} e^{-\zeta^2} \int_{-\pi/2}^{\pi/2} d\beta\, (\cos\beta)^{k+1}(\epsilon + 1 - e^{-\frac{\nu}{\zeta\cos\beta}\frac{X_1}{\epsilon}}) \\
& + 16X_1^{1/2} \int_{-\infty}^{\infty} dw \int_0^{\infty} d\eta \nu^{-1/2}\eta^{k+1/2} e^{-\eta^2-w^2} \\
\le & -4\ln X_1 \int_0^{\infty} d\zeta\, \nu^{-1}\zeta^{k+2} e^{-\zeta^2} \int_{-\pi/2}^{\pi/2} d\beta\, (\cos\beta)^{k+1}(\epsilon + \frac{\nu}{\zeta\cos\beta}\frac{X_1}{\epsilon}) \\
& + 16X_1^{1/2} \int_{-\infty}^{\infty} dw \int_0^{\infty} d\eta \nu^{-1/2}\eta^{k+1/2} e^{-\eta^2-w^2} \\
\le & -4\ln X_1 \int_0^{\infty} d\zeta\, \zeta^{k+1} e^{-\zeta^2} \pi\, (\epsilon\zeta\nu^{-1} + \frac{X_1}{\epsilon}) \\
& + 16X_1^{1/2} \int_{-\infty}^{\infty} dw \int_0^{\infty} d\eta \nu^{-1/2}\eta^{k+1/2} e^{-\eta^2-w^2}.
\end{aligned}
$$

By setting $\epsilon = X_1^{1/2}$, we have $|J| \lesssim X_1^{1/2}\ln X_1$, so that the last term of (13) remains finite.

[6] Obviously $G(x) \ge 0$ for $x \ge 0$. If we introduce $G_n(x) \equiv (1/n)x^n e^x - G(x)$ $(n > 0)$, then we have $G_1' = x^{-1}\{(x + x^2 - 1)e^x + 1\} \equiv x^{-1}g_1(x)$. Because $g_1' = (3x + x^2)e^x \ge 0$ and $g_1(0) = 0$, $g_1(x)$ is non-negative for $x \ge 0$. Therefore $G_1 \ge G_1(0) = 0$. Now compare $G_{1/2}$ with G_1. Because $G_{1/2} - G_1 = (2\sqrt{x} - x)e^x$, $G_{1/2} \ge G_1 \ge 0$ holds for $x \le 1$. For $x \ge 1$, $G_{1/2}' = x^{-1}\{(x^{1/2} + 2x^{3/2} - 1)e^x + 1\} \ge 0$ and thus $G_{1/2} \ge G_{1/2}(1) \ge G_1(1) \ge 0$. Thus we conclude $G_{1/2}(x) \ge 0$, i.e., $0 \le G(x) \le 2\sqrt{x}e^x$, for $x \ge 0$.

We thus conclude that the source term does not influence the diverging rate of the gradient $\left(I^{k,\ell,m}\right)'$ in (13).

2.2.2 Over a convex surface

Consider the problem

$$\zeta_1\frac{\partial\phi}{\partial x_1}+\zeta_2\frac{\partial\phi}{\partial x_2}=-\nu\phi+S,$$
$$\phi=\begin{cases}g_+(\theta,\boldsymbol{\zeta}), & \boldsymbol{\zeta}\cdot\boldsymbol{n}(r=1,\theta)>0,\\ g_-(\theta,\boldsymbol{\zeta}), & \boldsymbol{\zeta}\cdot\boldsymbol{n}(r=R,\theta)>0,\end{cases}$$

which is obtained by adding the source S to the equation of problem (5). Here, we suppose that $S(x_1,x_2,\boldsymbol{\zeta})$ behaves in the same way as the moments of ϕ for the partial model. We use the same notation as in Sect. 2.1.2, see Fig. 1(a).

The solution in the range $|\alpha|<\alpha_*$ and its moment on the positive x_1-axis are again of our present interest; the former is written as

$$\phi(x_1,0,\boldsymbol{\zeta})=g_+(\theta_w,\alpha_w,\eta,w)e^{-\frac{\nu s}{\eta}}+\int_0^s\frac{1}{\eta}e^{-\frac{\nu}{\eta}(s-t)}S(\tilde{x},\tilde{y},\boldsymbol{\zeta})dt,$$

where $\tilde{x}=x_w+t\cos\alpha$, $\tilde{y}=y_w+t\sin\alpha$, and the partial-range moments to be considered on the x_1-axis are written as

$$\begin{aligned}I[S]\equiv&\int_{-\infty}^{\infty}dw\int_0^{\infty}d\eta\,\eta\int_{-\alpha_*}^{\alpha_*}d\alpha\,\eta^k\cos^\ell\alpha\,\sin^m\alpha\,\phi e^{-\eta^2-w^2}\\
=&\int_{-\infty}^{\infty}dw\int_0^{\infty}d\eta\int_{-\alpha_*}^{\alpha_*}d\alpha\,\eta^{k+1}\cos^\ell\alpha\,\sin^m\alpha\,g_+(\theta_w,\alpha_w,\eta,w)e^{-\eta^2-w^2-\frac{\nu}{\eta}s}\\
&+\int_{-\infty}^{\infty}dw\int_0^{\infty}d\eta\int_{-\alpha_*}^{\alpha_*}d\alpha\,\eta^k\cos^\ell\alpha\,\sin^m\alpha\,e^{-\eta^2-w^2}\int_0^s e^{-\frac{\nu}{\eta}(s-t)}S(\tilde{x},\tilde{y},\boldsymbol{\zeta})dt.\end{aligned}$$

The difference from the partial model case is the second term in the above, i.e., the partial model case is recovered by the above notation as $I[0]$. Then, denoting the derivative in x_1 by $'$, we have

$$\begin{aligned}I'[S]=&I'[0]+\int_{-\infty}^{\infty}dw\int_0^{\infty}d\eta\,\alpha_*'\,\eta^k\cos^\ell\alpha_*\,\sin^m\alpha_*\,e^{-\eta^2-w^2}\\
&\times\int_0^{s_*}e^{-\frac{\nu}{\eta}(s_*-t)}[S(\tilde{x}_*,\tilde{y}_*,\alpha_*,\eta,w)+(-1)^mS(\tilde{x}_*,-\tilde{y}_*,-\alpha_*,\eta,w)]dt\\
&+\int_{-\infty}^{\infty}dw\int_0^{\infty}d\eta\int_{-\alpha_*}^{\alpha_*}d\alpha\,\eta^k\cos^\ell\alpha\,\sin^m\alpha\,e^{-\eta^2-w^2}s'S(x_1,0,\boldsymbol{\zeta})\\
&-\int_{-\infty}^{\infty}dw\int_0^{\infty}d\eta\int_{-\alpha_*}^{\alpha_*}d\alpha\,\eta^k\cos^\ell\alpha\,\sin^m\alpha\,e^{-\eta^2-w^2}s'\frac{\nu}{\eta}\int_0^s e^{-\frac{\nu}{\eta}(s-t)}S(\tilde{x},\tilde{y},\boldsymbol{\zeta})dt\\
&+\int_{-\infty}^{\infty}dw\int_0^{\infty}d\eta\int_{-\alpha_*}^{\alpha_*}d\alpha\,\eta^k\cos^\ell\alpha\,\sin^m\alpha\,e^{-\eta^2-w^2}\\
&\quad\times\int_0^s e^{-\frac{\nu}{\eta}(s-t)}(x_w'\partial_1S+y_w'\partial_2S)dt\end{aligned}$$

$$
\begin{aligned}
=&I'[0]+\int_{-\infty}^{\infty}dw\int_0^{\infty}d\eta\,\eta^k\cos^{\ell}\alpha_*\,\sin^m\alpha_*\,\alpha_*'\,e^{-\eta^2-w^2}\\
&\times\int_0^{s_*}e^{-\frac{\nu}{\eta}(s_*-t)}[S(\tilde{x}_*,\tilde{y}_*,\alpha_*,\eta,w)+(-1)^mS(\tilde{x}_*,-\tilde{y}_*,-\alpha_*,\eta,w)]dt\\
&+\int_{-\infty}^{\infty}dw\int_0^{\infty}d\eta\int_{-\alpha_*}^{\alpha_*}d\alpha\,\eta^k\cos^{\ell}\alpha\,\sin^m\alpha\,e^{-\eta^2-w^2}s'S(x_1,0,\boldsymbol{\zeta})\\
&-\int_{-\infty}^{\infty}dw\int_0^{\infty}d\eta\int_{-\alpha_*}^{\alpha_*}d\alpha\,\eta^k\cos^{\ell}\alpha\,\sin^m\alpha\,e^{-\eta^2-w^2}s'\\
&\times\{\int_0^s\partial_t[e^{-\frac{\nu}{\eta}(s-t)}S(\tilde{x},\tilde{y},\boldsymbol{\zeta})]dt-\int_0^s e^{-\frac{\nu}{\eta}(s-t)}(\cos\alpha\partial_1S+\sin\alpha\partial_2S)dt\}\\
&+\int_{-\infty}^{\infty}dw\int_0^{\infty}d\eta\int_{-\alpha_*}^{\alpha_*}d\alpha\,\eta^k\cos^{\ell}\alpha\,\sin^m\alpha\,e^{-\eta^2-w^2}\\
&\quad\times\int_0^s e^{-\frac{\nu}{\eta}(s-t)}(x_w'\partial_1S+y_w'\partial_2S)dt\\
=&I'[0]+\int_{-\infty}^{\infty}dw\int_0^{\infty}d\eta\,\eta^k\cos^{\ell}\alpha_*\,\sin^m\alpha_*\,\alpha_*'\,e^{-\eta^2-w^2}\\
&\times\int_0^{s_*}e^{-\frac{\nu}{\eta}(s_*-t)}[S(\tilde{x}_*,\tilde{y}_*,\alpha_*,\eta,w)+(-1)^mS(\tilde{x}_*,-\tilde{y}_*,-\alpha_*,\eta,w)]dt\\
&+\int_{-\infty}^{\infty}dw\int_0^{\infty}d\eta\int_{-\alpha_*}^{\alpha_*}d\alpha\,\eta^k\cos^{\ell}\alpha\,\sin^m\alpha\,e^{-\eta^2-w^2-\frac{\nu}{\eta}s}s'S(x_w,y_w,\boldsymbol{\zeta})\\
&+\int_{-\infty}^{\infty}dw\int_0^{\infty}d\eta\int_{-\alpha_*}^{\alpha_*}d\alpha\,\eta^k\cos^{\ell}\alpha\,\sin^m\alpha\,e^{-\eta^2-w^2}\int_0^s e^{-\frac{\nu}{\eta}(s-t)}\partial_1Sdt\\
=&I'[0]-\int_{-\infty}^{\infty}dw\int_0^{\infty}d\eta\,\eta^k\cos^{\ell-1}\alpha_*\,\sin^{m+2}\alpha_*\,e^{-\eta^2-w^2}\\
&\times\int_0^{s_*}e^{-\frac{\nu}{\eta}(s_*-t)}[S(\tilde{x}_*,\tilde{y}_*,\alpha_*,\eta,w)+(-1)^mS(\tilde{x}_*,-\tilde{y}_*,-\alpha_*,\eta,w)]dt\\
&+\int_{-\infty}^{\infty}dw\int_0^{\infty}d\eta\int_{-\alpha_*}^{\alpha_*}d\alpha\,\eta^k\frac{\cos^{\ell}\alpha\,\sin^{m+1}\alpha}{(1-x_1^2\sin^2\alpha)^{1/2}}\\
&\qquad\times e^{-\eta^2-w^2-\frac{\nu}{\eta}s}x_1\sin\alpha S(x_w,y_w,\boldsymbol{\zeta})\\
&+\int_{-\infty}^{\infty}dw\int_0^{\infty}d\eta\int_{-\alpha_*}^{\alpha_*}d\alpha\,\eta^k\cos^{\ell+1}\alpha\,\sin^m\alpha\,e^{-\eta^2-w^2-\frac{\nu}{\eta}s}S(x_w,y_w,\boldsymbol{\zeta})\\
&+\int_{-\infty}^{\infty}dw\int_0^{\infty}d\eta\int_{-\alpha_*}^{\alpha_*}d\alpha\,\eta^k\cos^{\ell}\alpha\,\sin^m\alpha\,e^{-\eta^2-w^2}\int_0^s e^{-\frac{\nu}{\eta}(s-t)}\partial_1Sdt,
\end{aligned}
$$

where $\tilde{x}_*=x_{w*}+t\cos\alpha_*$ and $\tilde{y}_*=y_{w*}+t\sin\alpha_*$. Note that all the terms above, except for the last, are of the same type as those occurring in $I'[0]$. After a few manipulations, we have the following final form

$$
\begin{aligned}
I'[S]=&-x_1^{-(m+\ell+1)}(x_1^2-1)^{\frac{\ell-1}{2}}\{I_{\rm cv}^{k+1,m}(x_1)+\tilde{I}_{\rm cv}^{k,m}(x_1)\}\\
&+J_{\rm cv}^{k,\ell,m+1}[-\eta(\partial_1g_+-\partial_2g_+)+x_1\sin\alpha\{-\nu g_++S(x_w,y_w,\boldsymbol{\zeta})\}]
\end{aligned}
$$

$$
\begin{aligned}
&+\int_{-\infty}^{\infty}dw\int_{0}^{\infty}d\eta\int_{-\alpha_*}^{\alpha_*}d\alpha\,\eta^k\cos^{\ell+1}\alpha\,\sin^m\alpha\\
&\qquad\times e^{-\eta^2-w^2-\frac{\nu}{\eta}s}\{-\nu g_+ + S(x_w,y_w,\boldsymbol{\zeta})\}\\
&+\int_{-\infty}^{\infty}dw\int_{0}^{\infty}d\eta\int_{-\alpha_*}^{\alpha_*}d\alpha\,\eta^k\cos^{\ell}\alpha\,\sin^m\alpha\,e^{-\eta^2-w^2}\int_0^s e^{-\frac{\nu}{\eta}(s-t)}\partial_1 S dt,
\end{aligned}
\tag{14}
$$

where

$$
\begin{aligned}
\tilde{I}^{k,m}_{\rm cv}(x_1)=\int_{-\infty}^{\infty}dw\int_0^{\infty}d\eta\,\eta^k e^{-\eta^2-w^2}\int_0^{s_*}e^{-\frac{\nu}{\eta}(s_*-t)}\\
\times[S(\tilde{x}_*,\tilde{y}_*,\alpha_*,\eta,w)+(-1)^m S(\tilde{x}_*,-\tilde{y}_*,-\alpha_*,\eta,w)]dt.
\end{aligned}
$$

Because the behavior of the first three terms of (14) is known by the analyses for the partial model, the remaining task is to estimate the behavior of the last term of (14) by taking into account that the derivative of S with respect to the radial direction may diverge with the rate $1/\sqrt{r-1}$. Because

$$
|\partial_1 S|=|\partial_1 r\partial_r S+\partial_1\theta\partial_\theta S|=|\cos\theta\partial_r S-(\sin\theta/r)\partial_\theta S|\lesssim\frac{C}{\sqrt{r-1}},
$$

with some positive constant C, we evaluate the behavior of the last term of (14) by considering the following integral:

$$
\begin{aligned}
&|\int_{-\infty}^{\infty}dw\int_0^{\infty}d\eta\int_{-\alpha_*}^{\alpha_*}d\alpha\,\eta^k\cos^{\ell}\alpha\,\sin^m\alpha\,e^{-\eta^2-w^2}\int_0^s e^{-\frac{\nu}{\eta}(s-t)}\frac{1}{\sqrt{r-1}}dt|\\
\le&\int_{-\infty}^{\infty}dw\int_0^{\infty}d\eta\int_{-\alpha_*}^{\alpha_*}d\alpha\,\eta^k e^{-\eta^2-w^2}\int_0^s\frac{e^{-\frac{\nu}{\eta}(s-t)}\sqrt{r+1}}{\sqrt{t^2+2t\cos(\theta_w-\alpha)}}dt\\
\le&\sqrt{\pi(R+1)}\int_0^{\infty}d\eta\int_{-\alpha_*}^{\alpha_*}d\alpha\,\frac{\eta^k e^{-\eta^2}}{\sqrt{2\cos(\theta_w-\alpha)}}\int_0^s\frac{1}{\sqrt{t}}dt\\
=&\sqrt{2\pi(R+1)}\int_0^{\infty}d\eta\int_{-\alpha_*}^{\alpha_*}d\alpha\,\frac{\eta^k e^{-\eta^2}\sqrt{s}}{\sqrt{\cos\alpha_w}}\\
\le&4\sqrt{\pi R x_1}(\int_0^{\infty}\eta^k e^{-\eta^2}d\eta)\int_0^{\alpha_*}\frac{d\alpha}{\sqrt{x_1\cos\alpha-s}}\\
=&4\sqrt{\pi R x_1}(\int_0^{\infty}\eta^k e^{-\eta^2}d\eta)\int_0^{\alpha_*}\frac{d\alpha}{(1-x_1^2\sin^2\alpha)^{1/4}}\\
=&4\sqrt{\pi R x_1}(\int_0^{\infty}\eta^k e^{-\eta^2}d\eta)\int_0^{1}\frac{d\mu}{(1-\mu^2)^{1/4}(x_1^2-\mu^2)^{1/2}}\\
\le&4\sqrt{\pi R x_1}(\int_0^{\infty}\eta^k e^{-\eta^2}d\eta)\int_0^{1}\frac{d\mu}{(1-\mu)^{3/4}}=16\sqrt{\pi R x_1}(\int_0^{\infty}\eta^k e^{-\eta^2}d\eta),
\end{aligned}
$$

which remains finite as $x_1\searrow 1$.

Therefore, we conclude that the source term does not change the structure of the occurrence of diverging gradient.

2.2.3 Over a concave surface

Consider the problem

$$\zeta_1\frac{\partial\phi}{\partial x_1}+\zeta_2\frac{\partial\phi}{\partial x_2}=-\nu\phi+S,\qquad \text{b.c. } \phi=g_-(\theta,\boldsymbol{\zeta}),\ \boldsymbol{\zeta}\cdot\boldsymbol{n}(r=1,\theta)<0, \quad (15)$$

which is obtained by adding the source S to the equation of (7). Here, we suppose that $S(x_1,x_2,\boldsymbol{\zeta})$ behaves in the same way as the moments of ϕ for the partial model. We use the same notation as in Sect. 2.1.3, see Fig. 1(b).

The solution and its moments on the positive x_1-axis are again of our interest; the former is written as

$$\phi(x_1,0,\boldsymbol{\zeta})=g_-(\theta_w,\alpha_w,\eta,w)e^{-\frac{\nu s}{\eta}}+\int_0^s\frac{1}{\eta}e^{-\frac{\nu}{\eta}(s-t)}S(\tilde{x},\tilde{y},\boldsymbol{\zeta})dt, \quad (16)$$

while the latter are

$$\begin{aligned}I[S]\equiv&\langle\eta^k\,\cos^\ell\alpha\,\sin^m\alpha\,\phi\rangle\\=&\int_{-\infty}^{\infty}dw\int_0^{\infty}d\eta\int_{-\pi}^{\pi}d\alpha\,\eta^{k+1}\cos^\ell\alpha\,\sin^m\alpha\,g_-(\theta_w,\alpha_w,\eta,w)\,e^{-\eta^2-w^2-\frac{\nu}{\eta}s}\\&+\int_{-\infty}^{\infty}dw\int_0^{\infty}d\eta\int_{-\pi}^{\pi}d\alpha\,\eta^k\cos^\ell\alpha\,\sin^m\alpha\,e^{-\eta^2-w^2}\int_0^s e^{-\frac{\nu}{\eta}(s-t)}S(\tilde{x},\tilde{y},\boldsymbol{\zeta})dt,\end{aligned}$$

where $\tilde{x}=x_w+t\cos\alpha$ and $\tilde{y}=y_w+t\sin\alpha$. The difference from the partial model case is the second term; the first term, which we shall denote by $I[0]$ below, represents the corresponding moments for the partial model. Denoting the derivative in x_1 by $'$, we have

$$\begin{aligned}I'[S]=&I'[0]+\int_{-\infty}^{\infty}dw\int_0^{\infty}d\eta\int_{-\pi}^{\pi}d\alpha\,\eta^k\cos^\ell\alpha\,\sin^m\alpha\,e^{-\eta^2-w^2}s'S(x_1,0,\boldsymbol{\zeta})\\&+\int_{-\infty}^{\infty}dw\int_0^{\infty}d\eta\int_{-\pi}^{\pi}d\alpha\,(-\nu/\eta)\eta^k\cos^\ell\alpha\,\sin^m\alpha\\&\qquad\times e^{-\eta^2-w^2}s'\int_0^s e^{-\frac{\nu}{\eta}(s-t)}S(\tilde{x},\tilde{y},\boldsymbol{\zeta})dt\\&+\int_{-\infty}^{\infty}dw\int_0^{\infty}d\eta\int_{-\pi}^{\pi}d\alpha\,\eta^k\cos^\ell\alpha\,\sin^m\alpha\,e^{-\eta^2-w^2}\\&\qquad\times\int_0^s e^{-\frac{\nu}{\eta}(s-t)}(x'_w\partial_1S+y'_w\partial_2S)dt\\=&I'[0]+\int_{-\infty}^{\infty}dw\int_0^{\infty}d\eta\int_{-\pi}^{\pi}d\alpha\,\eta^k\cos^\ell\alpha\,\sin^m\alpha\,e^{-\eta^2-w^2}s'\\&\qquad\times\{e^{-\frac{\nu}{\eta}s}S(x_w,y_w,\boldsymbol{\zeta})+\int_0^s e^{-\frac{\nu}{\eta}(s-t)}\partial_tS(\tilde{x},\tilde{y},\boldsymbol{\zeta})dt\}\\&+\int_{-\infty}^{\infty}dw\int_0^{\infty}d\eta\int_{-\pi}^{\pi}d\alpha\,\eta^k\cos^\ell\alpha\,\sin^m\alpha\,e^{-\eta^2-w^2}\\&\qquad\times\int_0^s e^{-\frac{\nu}{\eta}(s-t)}(x'_w\partial_1S+y'_w\partial_2S)dt\end{aligned}$$

$$
\begin{aligned}
=&I'[0]+\int_{-\infty}^{\infty}dw\int_0^{\infty}d\eta\int_{-\pi}^{\pi}d\alpha\,\eta^k\cos^{\ell}\alpha\,\sin^m\alpha\\
&\times e^{-\eta^2-w^2}s'e^{-\frac{\nu}{\eta}s}S(x_w,y_w,\boldsymbol{\zeta})\\
&+\int_{-\infty}^{\infty}dw\int_0^{\infty}d\eta\int_{-\pi}^{\pi}d\alpha\,\eta^k\cos^{\ell}\alpha\,\sin^m\alpha\,e^{-\eta^2-w^2}\int_0^s e^{-\frac{\nu}{\eta}(s-t)}\partial_1 S dt\\
=&I'[0]-\int_{-\infty}^{\infty}dw\int_0^{\infty}d\eta\int_{-\pi}^{\pi}d\alpha\,\eta^k\frac{\cos^{\ell}\alpha\,\sin^{m+1}\alpha}{(1-x_1^2\sin^2\alpha)^{1/2}}e^{-\eta^2-w^2-\frac{\nu}{\eta}s}\\
&\times x_1\sin\alpha S(x_w,y_w,\boldsymbol{\zeta})\\
&+\int_{-\infty}^{\infty}dw\int_0^{\infty}d\eta\int_{-\pi}^{\pi}d\alpha\,\eta^k\cos^{\ell+1}\alpha\,\sin^m\alpha\,e^{-\eta^2-w^2-\frac{\nu}{\eta}s}S(x_w,y_w,\boldsymbol{\zeta})\\
&+\int_{-\infty}^{\infty}dw\int_0^{\infty}d\eta\int_{-\pi}^{\pi}d\alpha\,\eta^k\cos^{\ell}\alpha\,\sin^m\alpha\,e^{-\eta^2-w^2}\int_0^s e^{-\frac{\nu}{\eta}(s-t)}\partial_1 S dt.
\end{aligned}
$$

Here the second and third terms are of the same type as $I'[0]$ and induce the same singularity as the partial model case. For later convenience, we rewrite the result as

$$
\begin{aligned}
I'[S]=&J_{\rm cc}^{k,\ell,m+1}[\eta(\partial_1 g_- -\partial_2 g_-)-x_1\sin\alpha\{-\nu g_- +S(x_w,y_w,\boldsymbol{\zeta})\}]\\
&+\int_{-\infty}^{\infty}dw\int_0^{\infty}d\eta\int_{-\pi}^{\pi}d\alpha\,\eta^k\cos^{\ell+1}\alpha\,\sin^m\alpha\\
&\quad\times e^{-\eta^2-w^2-\frac{\nu}{\eta}s}[-\nu g_- +S(x_w,y_w,\boldsymbol{\zeta})]\\
&+\int_{-\infty}^{\infty}dw\int_0^{\infty}d\eta\int_{-\pi}^{\pi}d\alpha\,\eta^k\cos^{\ell}\alpha\,\sin^m\alpha\,e^{-\eta^2-w^2}\int_0^s e^{-\frac{\nu}{\eta}(s-t)}\partial_1 S dt. \quad (17)
\end{aligned}
$$

The remaining task is thus to estimate the behavior of the last term of (17). By taking into account that the derivative of $S(x,y,\boldsymbol{\zeta})$ with respect to $r=(x^2+y^2)^{1/2}$ may diverge with the rate $\ln(1-r)$ if $r\nearrow 1$. Because $\partial_1 S$ is taken along the path $(x_1,x_2)=(\tilde{x},\tilde{y})$, $r=(\tilde{x}^2+\tilde{y}^2)^{1/2}$ in the present case, we have

$$
\begin{aligned}
|\partial_1 S|=&|\partial_1 r\partial_r S+\partial_1\theta\partial_\theta S|=|\cos\theta\partial_r S-(\sin\theta/r)\partial_\theta S|\\
&\lesssim -C\ln(1-r)\le -C\ln(1-r^2)+C\ln 2=-C\ln[-t(t+2\cos\alpha_w)/2].
\end{aligned}
$$

We thus evaluate the last term by considering the following integral:

$$
\begin{aligned}
&|\int_{-\infty}^{\infty}dw\int_0^{\infty}d\eta\int_{-\pi}^{\pi}d\alpha\,\eta^k\cos^{\ell}\alpha\,\sin^m\alpha\,e^{-\eta^2-w^2}\int_0^s e^{-\frac{\nu}{\eta}(s-t)}\ln[-t(t+2\cos\alpha_w)]dt|\\
\le&-\int_{-\infty}^{\infty}dw\int_0^{\infty}d\eta\int_{-\pi}^{\pi}d\alpha\,\eta^k e^{-\eta^2-w^2}\int_0^s[\ln t+\ln(-t-2\cos\alpha_w)]dt\\
=&-\sqrt{\pi}\int_0^{\infty}d\eta\,\eta^k e^{-\eta^2}\int_{-\pi}^{\pi}d\alpha\{s(\ln s-1)\\
&+(s+2\cos\alpha_w)[\ln(-s-2\cos\alpha_w)-1]-2\cos\alpha_w[\ln(-2\cos\alpha_w)-1]\}.
\end{aligned}
$$

Here we have taken into account that $0 \le -t(t+2\cos\alpha_w) = 1-r^2 \le 1$. Since $x\ln x$ is bounded for $0 \le x \le 2$, the integrand is bounded, and the last term (17) remains finite as $x_1 \nearrow 1$.

We thus conclude that the source term does not influence the structure of the occurrence of diverging gradient.

2.3 Discussions

From the analyses in Sects. 2.1 and 2.2, it is now clear that the essence of the singularities has already been embedded in the partial model. They are confined in $J^{k,-1,m}[\cdot]$ of (13), $J_{\rm cv}^{k,0,m+1}[\cdot]$ and $x_1^{-m-1}(x_1^2-1)^{-1/2}\{I_{\rm cv}^{k+1,m}(x_1)+\tilde{I}_{\rm cv}^{k,m}(x_1)\}$ of (14), and $J_{\rm cc}^{k,0,m+1}[\cdot]$ of (17) for the planar, convex and concave boundary, respectively, and are commonly identified as the divergence of the integrand for the molecular velocity nearly tangential to the boundary. Among them, the diverging rate of J's is commonly logarithmic, while that of $x_1^{-m-1}(x_1^2-1)^{-1/2}\{I_{\rm cv}^{k+1,m}(x_1)+\tilde{I}_{\rm cv}^{k,m}(x_1)\}$ is the inverse of the square root. The latter occurs only when the boundary is convex.

In the kinetic description, for instance in (2), the boundary data of the VDF are prescribed only for the molecules leaving the boundary, while the VDF is determined by the kinetic equation for the molecules arriving at the boundary. Consequently, the VDF data are mostly mismatched, making a jump discontinuity in molecular velocity space in the direction tangential to the boundary. In the convex boundary case, it propagates into the gas region along the molecular trajectory (i.e., the characteristics of the equation), which in turn causes the inverse square root singularity $x_1^{-m-1}(x_1^2-1)^{-1/2}\{I_{\rm cv}^{k+1,m}(x_1)+\tilde{I}_{\rm cv}^{k,m}(x_1)\}$ by the variation effect of α_* in approaching the boundary. In the planar boundary case, however, the jump discontinuity does not propagate into the gas, because its characteristics is never away from the boundary. In the concave boundary case, as is clear from (16), the VDF itself is continuous (except for $\eta = 0$). These explain the reason why the inverse square root singularity exclusively occurs in the convex boundary case.

In [13], the source of the logarithmic singularity in the planar case was identified as the jump discontinuity of the VDF on the boundary in the spatially one-dimensional setting. In the meantime, as is mentioned above, the jump discontinuity does not exist in the concave case. Nevertheless, the logarithmic singularity occurs commonly in the planar and concave cases. This seemingly puzzling situation can be understood if we closely observe the arguments of $J^{k,-1,m}[\cdot]$ of (13) and $J_{\rm cc}^{k,0,m+1}[\cdot]$ of (17). Let us take the latter for instance, i.e., $J_{\rm cc}^{k,0,m+1}[\eta\partial_1 g_- - \eta\partial_2 g_- - x_1\sin\alpha(-\nu g_- + S_w)]$, where $S_w = S(x_w, y_w, \boldsymbol{\zeta})$, and go back to (15). Then, the term $\zeta_2\partial\phi/\partial x_2$ in (15) on the positive x_1-axis can be written in terms of the cylindrical coordinates as

$$\zeta_2\frac{\partial\phi}{\partial x_2} = \frac{\eta\sin\alpha}{x_1}\frac{\partial\phi}{\partial\theta} - \frac{\eta\sin\alpha}{x_1}\frac{\partial\phi}{\partial\alpha},$$

where $\tan\theta = x_2/x_1$, $\tan(\alpha+\theta) = \zeta_2/\zeta_1$, and r has been replaced by x_1 because $\theta = 0$ on the positive x_1-axis. If we substitute the expression of $\phi(x_1, x_2, \boldsymbol{\zeta})$

corresponding to (16) into the right-hand side, we eventually obtain

$$\zeta_2\frac{\partial\phi}{\partial x_2} =\frac{\eta\sin\alpha}{x_1}\{(D\Theta_w)_0(\partial_1 g_- - \partial_2 g_-) - \frac{1}{\eta}\frac{\partial s}{\partial\alpha}(-\nu g_- + S_w)\}e^{-\frac{\nu}{\eta}s} + \sin\alpha\int_0^s e^{-\frac{\nu}{\eta}(s-t)}\partial_2 S(\tilde{x},\tilde{y},\boldsymbol{\zeta})dt,$$

where $\tan\Theta_w = [r\sin\theta - s\sin(\alpha+\theta)]/[r\cos\theta - s\cos(\alpha+\theta)]$, which is reduced to $\tan\theta_w$ when $\theta = 0$, and $(D\Theta_w)_0 = (\frac{\partial}{\partial\theta} - \frac{\partial}{\partial\alpha})\Theta_w\Big|_{\theta=0}$. By direct calculation, we see that

$$(D\Theta_w)_0 = x_1(x_1 - s\cos\alpha) + x_1\sin\alpha\frac{\partial s}{\partial\alpha},$$

and that

$$\begin{aligned}\zeta_2\frac{\partial\phi}{\partial x_2} =&\frac{1}{x_1^2}\frac{\partial s}{\partial\alpha}\{\eta(\partial_1 g_- - \partial_2 g_-) - x_1\sin\alpha(-\nu g_- + S_w)\}e^{-\frac{\nu}{\eta}s}\\ &+\{-\frac{1}{x_1^2}\frac{\partial s}{\partial\alpha}(1 - x_1^2\sin^2\alpha) + \sin\alpha(x_1 - s\cos\alpha)\}\eta(\partial_1 g_- - \partial_2 g_-)e^{-\frac{\nu}{\eta}s}\\ &+\sin\alpha\int_0^s e^{-\frac{\nu}{\eta}(s-t)}\partial_2 S(\tilde{x},\tilde{y},\boldsymbol{\zeta})dt. \qquad (18)\end{aligned}$$

Here, it is crucial to note that

$$\frac{\partial s}{\partial\alpha} = -x_1\sin\alpha\left(1 + \frac{x_1\cos\alpha}{(1 - x_1^2\sin^2\alpha)^{1/2}}\right),$$

is continuous if x_1 is strictly less than unity, but is discontinuous at $\alpha = \pm\pi/2$ in the limit $x_1 \to 1$. Due to this fact, the second and third terms on the right-hand side of (18) is continuous, while the first term has a jump discontinuity at $\alpha = \pm\pi/2$, i.e., the direction of molecular velocity tangential to the boundary. The part that actually generates the jump discontinuity in the first term in (18) is

$$-\frac{\cos\alpha\sin\alpha}{(1 - x_1^2\sin^2\alpha)^{1/2}}\{\eta(\partial_1 g_- - \partial_2 g_-) - x_1\sin\alpha(-\nu g_- + S_w)\}e^{-\frac{\nu}{\eta}s},$$

which is exactly the same, except for the factor $\cos\alpha$, as that occurs in $J_{\rm cc}^{k,0,m+1}[\eta\partial_1 g_- - \eta\partial_2 g_- - x_1\sin\alpha(-\nu g_- + S_w)]$.

The origin of $J^{k,-1,m}[\eta\sin\alpha\partial_1 g_- + \nu g_- - S_w]$, where $S_w = S(0, y_w, \boldsymbol{\zeta})$, in (13) for the planar boundary case can be discussed in the same way. Here, we shall take a short cut to explain it. Let us consider the difference of $\nu\phi + \zeta_2\partial\phi/\partial x_2$ between its left and right limit at $\alpha = \pi/2$. The limit from the right is given by $\nu g_- + \zeta_2\partial g_-/\partial x_2$, while the limit from the left is given by $\nu\phi + \zeta_2\partial\phi/\partial x_2 = S_w$. These are the consequence of the fact that the former is determined by the boundary data, while the latter is determined by solving the equation itself. Thus, their difference is given by

$$\nu(\phi - g_-) + \zeta_2\frac{\partial(\phi - g_-)}{\partial x_2} = -(\zeta_2\frac{\partial g_-}{\partial x_2} + \nu g_- - S_w).$$

The right-hand side is nothing else than the argument of $J^{k,-1,m}[\cdot]$ at $\alpha = \pi/2$, because $\zeta_2 \partial g_- / \partial x_2 = \zeta_2 \partial_1 g_- = \eta \sin\alpha \partial_1 g_-$. Therefore, the singularity is induced in the present case by both the jump discontinuity of the VDF itself and of its derivative. In particular, the latter may occur even in the collisionless case. We shall omit the similar discussion for the convex case, because $J^{k,0,m+1}_{\mathrm{cv}}[\cdot]$ is not dominant.

In this way, we have now reached a unified view that the singularities of our interest is the trace of the jump discontinuity of the VDF and/or its derivative in the direction tangential to the boundary.

3 From prototype to general smooth boundary

In the present section, we shall extend the results for planar and cylindrical convex/concave boundaries to general smooth boundaries.

The singularities that we have discussed in Sect. 2 are induced by the distribution of molecules that travel almost tangential to the boundary. Although the boundary geometry has been limited so far, we can apply the obtained results to more general geometry of the boundary, as far as it is smooth. This is because the free flight length of molecules traveling almost tangential to the boundary is determined by the local geometry of the boundary, when the position under consideration is close to the boundary. Its global arrangement or geometry does not affect the discussions developed in Sect. 2. We thus classify the points on the boundary by following the differential geometry of surfaces and discuss the singularity which is dominant there.

The local geometry of the surface is classified into four types. They are represented by the elliptic, hyperbolic, parabolic and flat umbilic points. The principal curvatures at a surface point are the maximum and minimum of the normal curvatures there, where the normal curvature is the curvature of the curve that is the intersection between the surface and the normal plane at the point. At elliptic points, the principal curvatures have the same sign, and thus the normal curvature in any tangential direction has the same sign. At hyperbolic points, the principal curvatures have opposite signs. At parabolic points, one of the principal curvatures is zero. At flat umbilic points (or level points), both principal curvatures are zero, so that the normal curvature in any tangential direction is zero. The key notion is that the surface can be locally approximated by a circle, or a quadratic polynomial, in the normal plane, if the normal curvature does not vanish.

(Case 1) at the elliptic point There are two possibilities: the boundary is convex or concave. If convex, the boundary on any normal plane is circular and the results for the cylindrical convex case in Sect. 2.2.2 apply. Therefore, the singularity of $1/\sqrt{s}$ manifests itself, where and hereinafter s is the normal distance from the boundary. If concave, the results for the cylindrical concave case in Sect. 2.2.3 apply, and the singularity of $\ln s$ manifests itself.

(Case 2) at the hyperbolic point There are two regions for the tangential directions: one is the region in which the normal curvature is always positive, another is the region in which the normal curvature is always negative. There are two tangential directions along which the normal curvature is zero. They are isolated and thus of measure zero in the tangential direction space. Then in the region of positive normal curvature the results for the cylindrical convex case apply, while in the region of negative normal curvature those for the cylindrical concave case apply. Thus, the singularity of $1/\sqrt{s}$ from the positive normal curvature side dominates.

(Case 3) at the parabolic point The normal curvature in any direction, except for one direction, is positive or negative. If positive, the results for the cylindrical convex case apply, and the singularity of $1/\sqrt{s}$ manifests itself. If negative, the results for the cylindrical concave case apply, and the singularity of $\ln s$ manifests itself. In fact, all the points on the inner and outer cylinder surfaces fall into this category. Since the direction of zero normal curvature is isolated, it does not contribute.

(Case 4) at the flat umbilic point The zero normal curvature in any direction does not necessarily mean that the surface is plane. For every fixed point on the smooth surface, we can assign a rectangular coordinates (x, y, z) whose origin is located at that point with the z axis normal to the surface; thus the x and y are the coordinates in the tangential plane. Then, in the vicinity of the point under consideration, the surface is expressed by the polynomial of x and y:

$$\begin{aligned} z &= c_{20}x^2 + c_{11}xy + c_{02}y^2 + c_{30}x^3 + c_{21}x^2y + c_{12}xy^2 + c_{03}y^3 + \cdots \\ &= \sum_{i+j=2}^{\infty} c_{ij}x^i y^j, \end{aligned}$$

where c_{ij} are constants $(i, j \geq 0)$. When at least one of c_{20}, c_{11}, and c_{02} is non-zero, the quadratic terms are dominant and the surface along the direction $\tan\theta = y/x$ is given by

$$z = (c_{20}\cos^2\theta + c_{11}\cos\theta\sin\theta + c_{02}\sin^2\theta)(x^2 + y^2) \equiv C_2(\theta)(x^2 + y^2).$$

When $C_2(\theta)$ is positive or negative for any θ, the point is elliptic. When the maximum and minimum of $C_2(\theta)$ have opposite sign, the point is hyperbolic. When the maximum or minimum of $C_2(\theta)$ is zero, the point is parabolic. Clearly, the quadratic terms vanish only at the isolated values of θ, when one of c_{20}, c_{11} and c_{02} is non-zero.

The flat umbilic point is the point where c_{20}, c_{11} and c_{02} are all zero [or equivalently $C_2(\theta)$ is identically zero]. Then, the cubic terms become dominant, as far as one of c_{30}, c_{21}, c_{12} and c_{03} is non-zero. In the case, $C_3(\theta) = \sum_{i=0}^{3} c_{i,3-i}\cos^i\theta\sin^{3-i}\theta$ can be zero at most at the isolated values of θ, and the case is reduced to the study of the canonical one $z = x^3$ in the x-z plane.

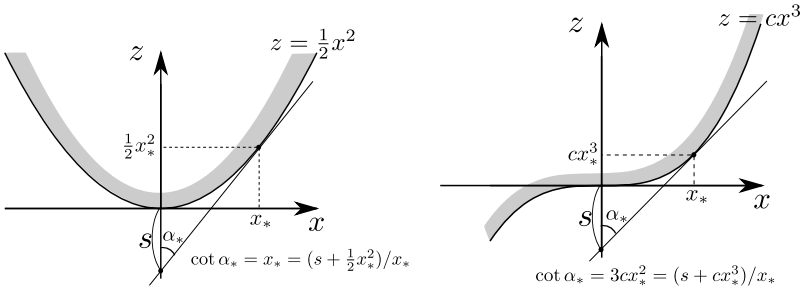

(a) Quadratic curve (b) Cubic curve

Fig. 2 Boundary shape and tangential direction.

When $C_2(\theta)$ and $C_3(\theta)$ are identically zero, then the quartic terms are dominant, as far as $C_4(\theta) = \sum_{i=0}^{4} c_{i,4-i} \cos^i\theta \sin^{4-i}\theta$ is not identically zero. Again, in this condition, $C_4(\theta)$ can be zero only at the isolated values of θ, and the case is reduced to the study of the canonical one $z = \pm x^4$ in the x-z plane. In this way, the study of the singularity at the flat umbilic point is reduced to the study of the vicinity of the surface $z = (\pm)^{n+1}x^n$, where $n \geq 3$ is an integer.

First consider the case that the surface is expressed by a cubic curve on a normal plane. There are two parts, one is convex and the other is concave. The concave side gives rise to the $\ln z$ singularity, which is concluded from the same argument as the cylindrical concave case in Sect. 2.2.3. On the other hand, at the convex side another singularity may arise, which can be estimated by a similar argument to the cylindrical convex case in Sect. 2.2.2. Here, the key difference is the contribution arising from the change of integration range, especially the change of the traveling direction of molecules tangential to the boundary. In the cylindrical convex case in Sects. 2.1.2 and 2.2.2, the canonical surface of which is quadratic, i.e., $z = (1/2)x^2$, the slope $\cot\alpha_*$ of the tangential line is given by $\cot\alpha_* = \sqrt{2s}$ [see Fig. 2(a)]. Thus we have a singularity proportional to $\partial\alpha_*/\partial s \sim -1/\sqrt{2s}$, which recovers the result in Sect. 2.1.2. The corresponding direction in the case of a cubic curve $z = cx^3$ (c: a positive constant) is given by the relation $\cot\alpha_* = 3cx_*^2 = (s + cx_*^3)/x_*$, where x_* is the x-coordinate of the point of tangency, from which the singularity proportional to $\partial\alpha_*/\partial s \sim -(2c/s)^{1/3}$ is induced [see Fig. 2(b)]. In general, the surface locally expressed by n-th polynomial $z = cx^n$ (c: a positive constant), the tangential direction is given by $\cot\alpha_* = ncx^{n-1} = (s + cx^n)/x$, which induces the singularity proportional to $\partial\alpha_*/\partial s \sim -((n-1)c/s)^{1/n}$. Note that when n is odd, this singularity occurs, but when n is even, the singularity of the negative fractional power occurs only when the curve is convex. When n is even and the curve is concave, the singularity $\ln s$ manifests itself. As $n \to \infty$, $\partial\alpha_*/\partial s \sim -((n-1)c/s)^{1/n} \to -1$ and the singularity degenerates. Then the singularity of fractional power, which is related to the propagation of discontinuity inside a gas, vanishes and the logarithmic singularity revives to be dominant.

4 Numerical demonstration

In the present section, we present some numerical results that support our discussions and conclusions so far. The numerical computations to confirm our assertion are really challenging, due to the necessity of the high accuracy near the boundary. We thus restrict ourselves to the case of the BGK model and/or the collisionless gas in the present paper. Numerical demonstration for the case of the original Boltzmann equation is left for future work.

Here we demonstrate the singularities on the parabolic and flat umbilic points. For the study of hyperbolic and elliptic points, spatially three dimensional study is inevitable, which is limited to the collisionless gas here.

4.1 Rarefied gas between coaxial circular cylinders

Consider a rarefied gas between coaxial circular cylinders with radii L and LR $(R > 1)$. The inner cylinder is at rest and kept at a uniform temperature T_0, while the outer is rotating with a circumferential velocity $(2\mathcal{R}T_0)^{1/2}u_w$ and is kept at a temperature $T_0(1+\tau_w)$, where $\mathcal{R}$ is the specific gas constant. Under the assumption that $|u_w| \ll 1$ and $|\tau_w| \ll 1$, the problem can be linearized and the behavior of a gas is described by the following linearized BGK equation and diffuse reflection boundary condition on the cylinder surfaces:

$$\zeta_r \frac{\partial \phi}{\partial r} + \frac{\zeta_\theta}{r}\frac{\partial \phi}{\partial \theta} + \zeta_z \frac{\partial \phi}{\partial z} + \frac{\zeta_\theta^2}{r}\frac{\partial \phi}{\partial \zeta_r} - \frac{\zeta_r \zeta_\theta}{r}\frac{\partial \phi}{\partial \zeta_\theta} = \mathcal{L}_{\mathrm{BGK}}[\phi],$$

$$\text{b.c. } \phi(r=1, \zeta_r > 0) = -2\pi^{1/2} \int_{\zeta_r<0} \zeta_r \phi E d\boldsymbol{\zeta},$$

$$\phi(r=R, \zeta_r < 0) = 2\pi^{1/2} \int_{\zeta_r>0} \zeta_r \phi E d\boldsymbol{\zeta} + 2\zeta_\theta u_w + (\zeta^2 - 2)\tau_w,$$

where (Lr, θ, Lz) is the spatial cylindrical coordinates, $(2\mathcal{R}T_0)^{1/2}(\zeta_r, \zeta_\theta, \zeta_z)$ is the corresponding coordinates for the molecular velocity, $\rho_0(2\mathcal{R}T_0)^{-3/2}[1 + \phi(r, \theta, z, \zeta_r, \zeta_\theta, \zeta_z)]E$ with $E = \pi^{-3/2}\exp(-\zeta^2)$ and $\zeta = (\zeta_r^2 + \zeta_\theta^2 + \zeta_z^2)^{1/2}$ is the velocity distribution function of gas molecules, $\mathcal{L}_{\mathrm{BGK}}[\phi]$ is the linearized collision operator for the BGK model, the specific form of which in the present case is given later. Below, we denote the density, temperature, flow velocity, stress tensor, and heat flow of the gas by $\rho_0(1+\omega)$, $T_0(1+\tau)$, $(2\mathcal{R}T_0)^{1/2}u_\alpha$, $p_0(\delta_{\alpha\beta} + P_{\alpha\beta})$, and $p_0(2\mathcal{R}T_0)^{1/2}Q_\alpha$, respectively, where $p_0 = \rho_0\mathcal{R}T_0$, $\{\alpha, \beta\} = \{r, \theta, z\}$ and $\delta_{\alpha\beta}$ is Kronecker's delta. They are defined as the moments of ϕ as follows:

$$\omega = \int \phi E d\boldsymbol{\zeta}, \quad u_\alpha = \int \zeta_\alpha \phi E d\boldsymbol{\zeta}, \quad \tau = \frac{2}{3}\int (\zeta^2 - \frac{3}{2})\phi E d\boldsymbol{\zeta}, \tag{19a}$$

$$P_{\alpha\beta} = 2\int \zeta_\alpha \zeta_\beta \phi E d\boldsymbol{\zeta}, \quad Q_\alpha = \int \zeta_\alpha (\zeta^2 - \frac{5}{2})\phi E d\boldsymbol{\zeta}. \tag{19b}$$

By the symmetry of the problem, u_z, Q_z, $P_{\theta z}$ and P_{rz} are all vanishing and will not be considered. $\mathcal{L}_{\rm BGK}[\phi]$ then takes the following reduced form:

$$\mathcal{L}_{\rm BGK}[\phi] = \frac{1}{k}\{-\phi + \omega + 2\zeta_r u_r + 2\zeta_\theta u_\theta + (\zeta^2 - \frac{3}{2})\tau\}.$$

where $k = (\sqrt{\pi}/2){\rm Kn}$. Here, Kn is the reference Knudsen number defined by the mean-free-path ℓ_0 at the resting equilibrium state with temperature T_0 and density ρ_0 divided by L, where ρ_0 is the average density of the gas between the cylinders.

Note that all the points on the boundary is the parabolic point in the present example. The inner cylinder is convex, while the outer cylinder is concave. In the numerical computations, we set $R = 2$. Before going further, keep in mind that, according to our results of discussions, the gradients of u_r, Q_r, P_{rr} and $P_{r\theta}$ with respect to r never diverge in approaching the boundary, while those of the others can diverge with the rate depending on whether the boundary is convex or not.

(Case I) Cylindrical Couette flow Let us set $\tau_w = 0$. This is nothing else than the Couette flow problem, which is axially symmetric, and all the quantities occurring in (19) are zero, except for u_θ, $P_{r\theta}$, and Q_θ. Their variation near the inner and outer cylinders for various k are shown in Fig. 3 as a function of the normal distance s from the boundaries, i.e., $s = r - 1$ near the inner and $s(= R - r) = 2 - r$ near the outer cylinder. As is clearly seen, the differences of u_θ and Q_θ from their values at the boundary change in proportion to $s^{1/2}$ near the inner and to $s \ln s$ near the outer cylinder as $s \to 0$, respectively. In contrast, the corresponding difference of $P_{r\theta}$ changes in proportion to s as $s \to 0$.[7] These are consistent with our theoretical predictions, not only on the diverging rate of the gradient (say, for u_θ and Q_θ) but also on the finiteness of the gradient of the moments which contain the multiplication of ζ_r in its definition (i.e., $P_{r\theta}$). Incidentally, in the present problem, Q_θ vanishes in the collisionless limit, and u_θ in the same limit behaves in the same way as $P_{r\theta}$ near the outer cylinder as is observed in the figure. The behavior of u_θ is due to that the boundary data along the outer cylinder surface is uniform and the dynamics that induces the logarithmic divergence in the collisionless gas is absent in the present case. Indeed, u_θ in the collisionless case is readily obtained as

$$\frac{u_\theta}{u_w} = \frac{r}{\pi R}(\pi + \frac{1}{r^2}\sqrt{r^2 - 1} - \arcsin\frac{1}{r}),$$

where $0 < \arcsin(1/r) < \pi/2$. Its gradient with respect to r is obviously finite as $r \to R$.

[7] In order to discriminate s against $s \ln s$, the quantities near the outer boundary are shown by the semi-log plot of the difference from the values on the boundary divided by the distance s. If the profile for small s is horizontal line, the difference grows in proportion to s near the boundary. If the profile for small s is a straight line with non-zero slope, the difference grows in proportion to $s \ln s$ near the boundary.

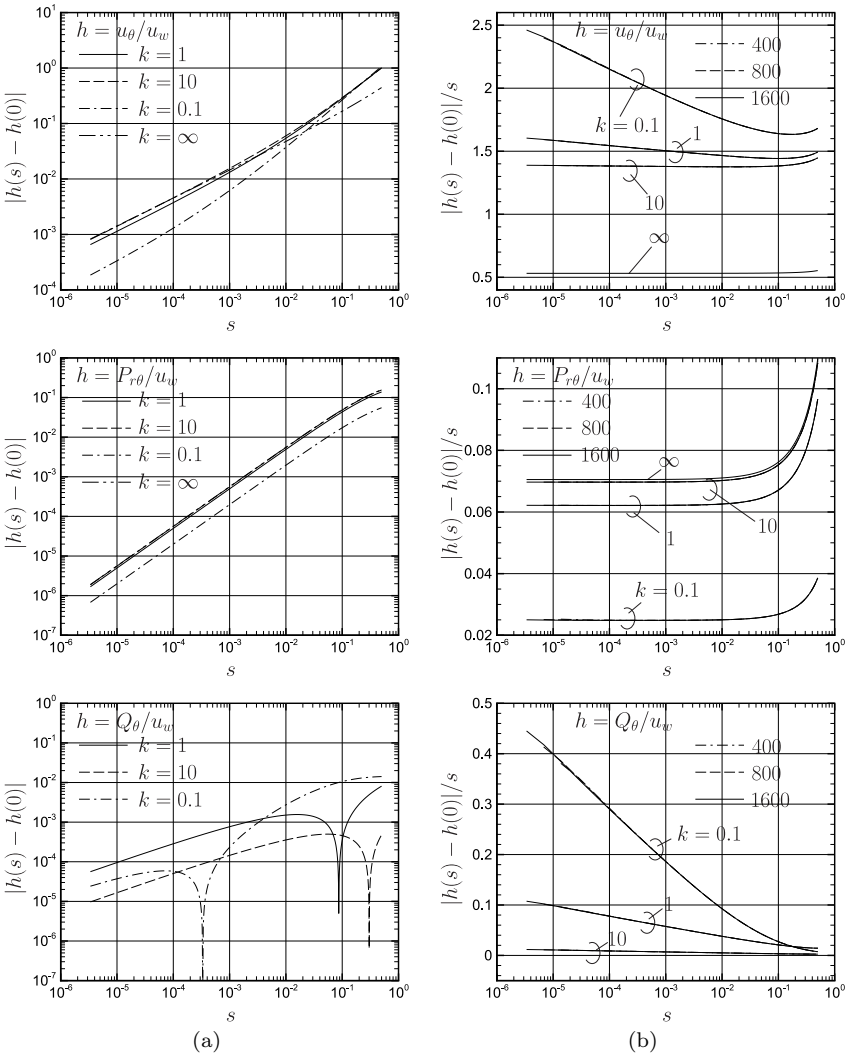

Fig. 3 Variations of u_θ, $P_{r\theta}$ and Q_θ as a function of the normal distance s in Case I. (a) Variations near the inner cylinder surface ($s = r - 1$). (b) Variations near the outer cylinder surface ($s = 2 - r$). In (b), the numbers in the legend are the number of grid intervals in r used in the computations.

(Case II) Flow induced by the nonuniform surface temperature

Let us set $u_w = 0$ and $\tau_w = a \sin\theta$, where a is a small constant. Since the surface temperature of the outer cylinder varies, the problem is no longer axially symmetric. However, a similarity solution can be applied, so that ω, u_r, τ, P_{rr}, $P_{\theta\theta}$, P_{zz} and Q_r are proportional to $\sin\theta$, while u_θ, $P_{r\theta}$ and Q_θ are proportional to $\cos\theta$. Here, we show the change of ω, u_r, τ and $P_{\theta\theta}$ divided by $\sin\theta$ and that of u_θ, $P_{r\theta}$ and Q_θ divided by $\cos\theta$ near the inner and outer

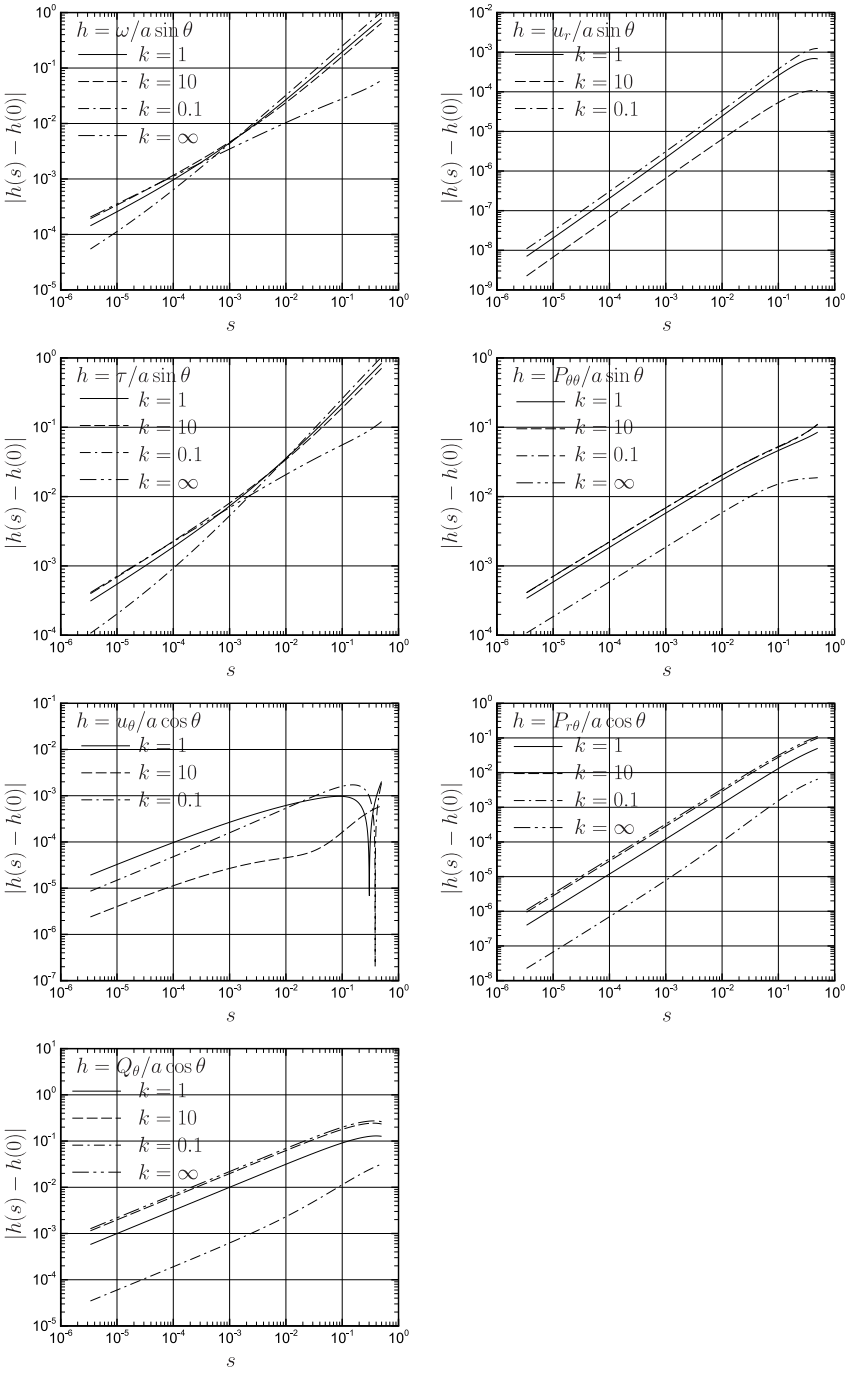

Fig. 4 Variations of ω, u_r, τ, $P_{\theta\theta}$, u_θ, $P_{r\theta}$ and Q_θ near the inner cylinder as a function of the normal distance $s(= r - 1)$ from the boundary in Case II.

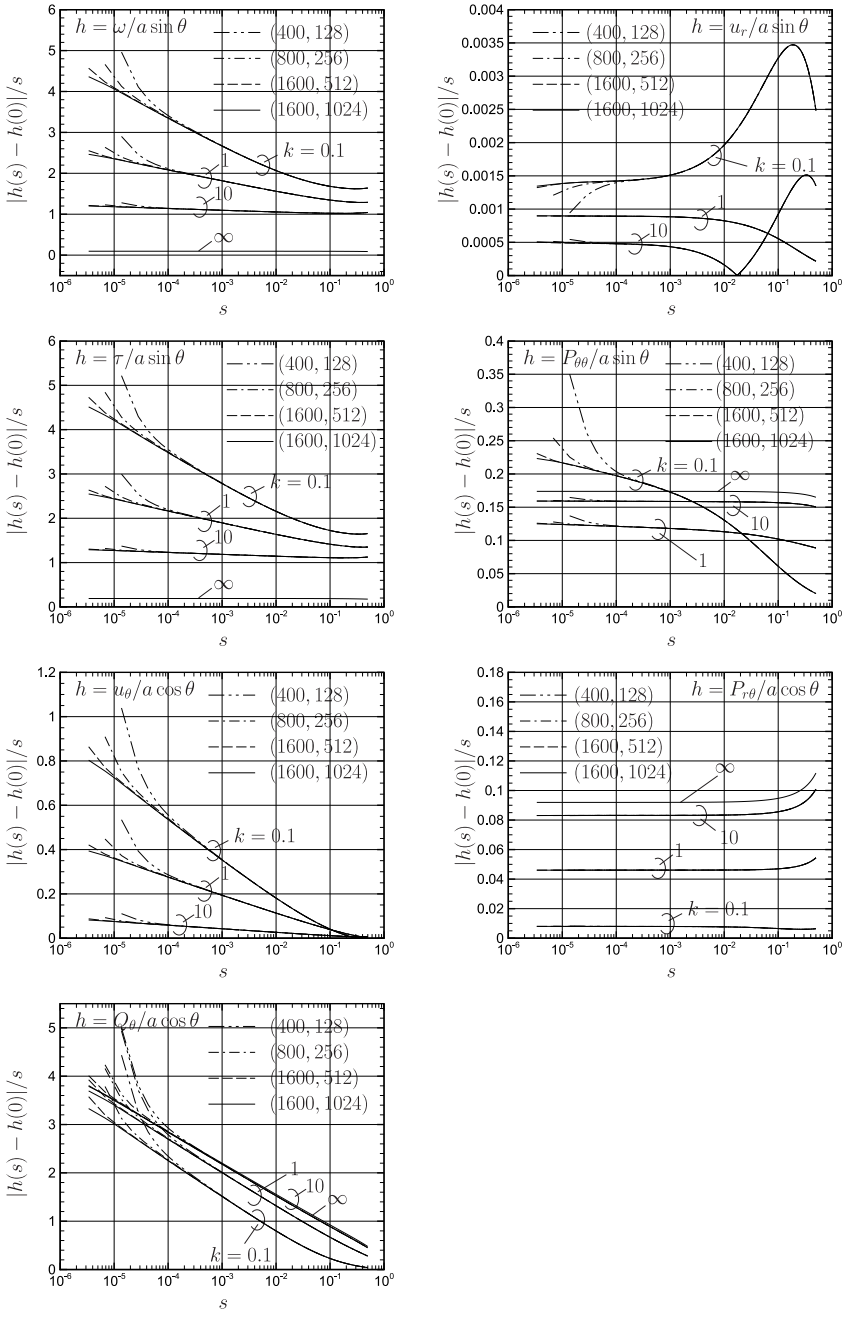

Fig. 5 Variations of ω, u_r, τ, $P_{\theta\theta}$, u_θ, $P_{r\theta}$ and Q_θ near the outer cylinder as a function of the normal distance $s(= 2 - r)$ from the boundary in Case II. The pairs of numbers in the legends are the pairs of the number of grid intervals in r and that in the azimuth angle of the molecular velocity, i.e., $\theta_\zeta = \arctan(\zeta_\theta/\zeta_r)$, for its half range.

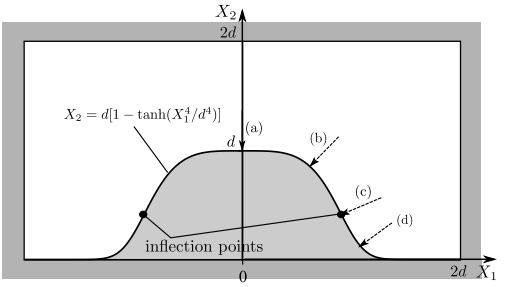

Fig. 6 Configuration of the surface with varying normal curvature. The X_1-coordinates of the surface positions pointed by the arrows (a)-(d) are as follows: (a) $X_1/d = 0$, (b) $X_1/d = 0.5994$, (c) $X_1/d = 0.8991$ and (d) $X_1/d = 1.1993$.

cylinders for various k in Figs. 4 and 5. As is clearly shown, u_r, $P_{r\theta}$, and Q_r change from their values at the boundary in proportion to s as $s \to 0$ both near the inner and outer cylinders. In contrast, the others (ω, τ, $P_{\theta\theta}$, u_θ and Q_θ) change from their values at the boundary in proportion to $s^{1/2}$ and $s \ln s$ as $s \to 0$ near the inner and outer cylinders, respectively. These are consistent with our theoretical predictions. Incidentally, in the collisionless case, $u_\theta \equiv 0$ and the gradients of all the other quantities, except for Q_θ, are readily seen to be finite at the outer cylinder. The gradient of Q_θ, however, diverges in proportion to $\ln s$ as $s \to 0$, which is in marked contrast to the behavior of u_θ in Case I. This is due to the effect of the boundary data variation along the outer cylinder surface, which is absent in Case I.

4.2 Thermally induced flow around a surface with varying normal curvature

The concerned surface with varying normal curvature consists of parabolic points and flat umbilic points (see Fig. 6). In the X_1-X_2 plane, the flat umbilic points are represented by three different points, one is $(X_1, X_2) = (0, d)$, and the others are the inflection points of the curve $X_2 = d[1 - \tanh(X_1^4/d^4)]$. The surface is locally approximated by a quartic curve at the former point, while it is approximated by a cubic curve at the latter, i.e., the inflection points. Except for the three flat-umbilic points, the surface is composed of parabolic points; the surface is convex between the inflection points and is concave elsewhere. The surface temperature is given by $T_w = T_0(1+\delta\tau_b)$ with $\tau_b = \frac{1}{2}(1+\cos(\frac{\pi X_1}{2d}))$ and $\delta \ll 1$. The outer square surface at $X_1 = \pm 2d$ and $X_2 = 2d$ is kept at the uniform reference temperature T_0. On the entire surface, the diffuse reflection is assumed. The quantities are to be made dimensionless in the same way as in Sect. 4.1 with d being the reference length in place of L and ρ_0 being the average density of the gas. Accordingly, s represents the (dimensional) normal distance divided by d and the reference Knudsen number in $k = (\sqrt{\pi}/2)\mathrm{Kn}$ is defined by the mean-free-path at the reference equilibrium state divided by d. The numerical computations have been carried out on the basis of the linearized BGK model as in Sect. 4.1.

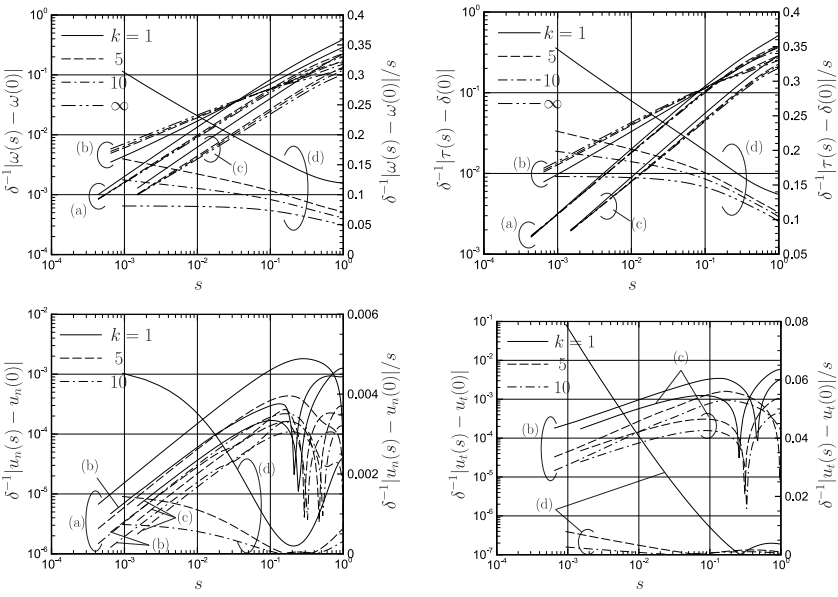

Fig. 7 Variations of ω, τ, u_n and u_t near the surface with varying curvature as a function of the normal distance s from the surface. The curves (a)-(d) in the figure indicate the results along the arrows (a)-(d) in Fig. 6. Note that the left vertical axis is for (a)-(c), while the right vertical axis is for (d).

Figure 7 shows the variations of density ω, temperature τ, flow velocity components u_n and u_t in the directions normal and tangential to the boundary near the representative surface points. As is clearly observed in the figure, ω, τ and u_t behave differently among the positions (a)-(c), while u_n behaves commonly among those positions. Here, it should be reminded that the left vertical axis in the figure is for (a)-(c)-plots, while the right vertical axis is for (d)-plot. The slope of the former for small s is 3/4, 1/2 and 2/3 for (a), (b) and (c), respectively, which implies the change in proportion to $s^{3/4}$, $s^{1/2}$ and $s^{2/3}$. Hence, the results are consistent with the theoretical predictions in Sect. 3. As for (d), the results are plotted against the right axis, and thus the straight line with non-zero slope implies the change in proportion to $s \ln s$, while the straight line with zero-slope implies the change in proportion to s. The density ω, temperature τ, tangential flow velocity u_t change commonly in proportion to $s \ln s$ for finite Knudsen numbers and tend to be proportional to s in the collisionless gas limit ($k = \infty$), though $u_t \equiv 0$ in the same limit. In the meantime, u_n tends to change in proportion to s as s becomes smaller. These observations are again consistent with the theoretical predictions for the parabolic points in Case 3 of Sect. 3. One may wonder if the regular behavior of ω and τ conflicts with our prediction. However, it should be noted that our theory does not exclude the possibility of the occurrence of cancellation of the singularity sources in the integrand as a result of integration. Actually, the

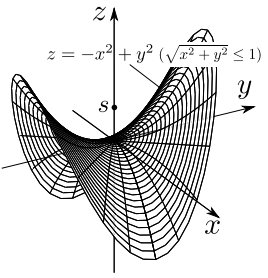

Fig. 8 The inner surface $z = -x^2 + (cy)^2$ with $x^2 + y^2 \le 1$ and $c = 1$.

similar situation does happen in the next example in Sect. 4.3. The numerical results are thus all consistent with our theory.

4.3 Collisionless gas near the saddle point of a surface

Consider a collisionless gas confined in a right circular cylinder with radius $2L$. Let us set the Cartesian space coordinates (Lx, Ly, Lz) in the way that the cylinder axis is in the z-direction and its surface is given by $x^2 + y^2 = 2^2$. Inside the cylinder, there is another surface, which we call the inner surface hereinafter, $z = -x^2 + c^2y^2$ with $x^2 + y^2 \le 1$, where $c \ge 1$ is a dimensionless constant, see Fig. 8. The cylinder is kept at temperature $T_0(1+\beta\cos\varphi)$, while the inner surface is kept at temperature $T_0(1+\beta r\cos\varphi)$. Here $\beta \ll 1$, $r = (x^2+y^2)^{1/2}$ and φ $(0 \le \varphi < 2\pi)$ is the polar angle in the x-y plane $(\tan\varphi = y/x)$. In this example, the origin of the spatial coordinates is the saddle point of the inner surface, a typical example of the hyperbolic point; see Case 2 in Sect. 3. Under the diffuse reflection condition on the boundaries, the velocity distribution function $\rho_0(2\mathcal{R}T_0)^{1/2}(1+\phi)E$ on the positive z-axis, where ρ_0 is a reference density, is obtained with the aid of the solution method in [7,8] in the form

$$\phi(0,0,z>0,\zeta,\theta_\zeta,\varphi_\zeta) = \begin{cases} \beta(\zeta^2-2)r_w\cos\varphi_w, & 0<\theta_\zeta<\theta_*, \\ \beta(\zeta^2-2)\cos\varphi_c, & \theta_*<\theta_\zeta<\pi, \end{cases} \tag{20}$$

where $(\zeta_x, \zeta_y, \zeta_z) = (\zeta\sin\theta_\zeta\cos\varphi_\zeta, \zeta\sin\theta_\zeta\sin\varphi_\zeta, \zeta\cos\theta_\zeta)$ is the molecular velocity divided by $(2\mathcal{R}T_0)^{1/2}$, and r_w, φ_w, φ_c and θ_* occurring in (20) are given as follows:

$$r_w = \frac{-\cot\theta_\zeta + (\cot^2\theta_\zeta + 4C(\varphi_w)z)^{1/2}}{2C(\varphi_w)},$$

$$\varphi_w = \varphi_\zeta + \pi \pmod{2\pi}, \quad \varphi_c = \varphi_\zeta + \pi \pmod{2\pi},$$

$$\cot\theta_* = \begin{cases} \cot\theta_t = 2(|C(\varphi_\zeta)|z)^{1/2}, & \varphi_\zeta \in [\varphi_*, \pi-\varphi_*) \cup [\pi+\varphi_*, 2\pi-\varphi_*), \\ \cot\theta_e = z - C(\varphi_\zeta), & \text{otherwise}, \end{cases}$$

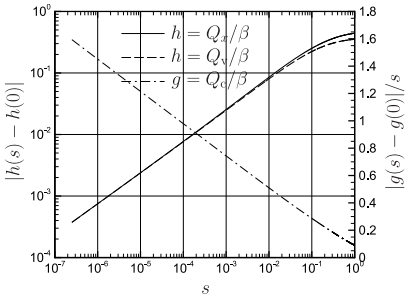

(a) Double-log and semi-log plots in the case of $c = 1$

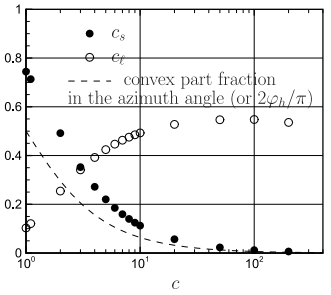

(b) Fraction of the convex part and magnitude of singularities for various values of c

Fig. 9 The x-component of heat flow Q_x, contributions to it from the convex part Q_v and from the concave part Q_c near the saddle point.

where

$$C(\varphi) = -\cos^2\varphi + c^2\sin^2\varphi,$$
$$\varphi_* = \frac{1}{2}\arccos\left(\frac{c^2 - 1 + 2z}{1 + c^2}\right) \le \frac{1}{2}\arccos\left(\frac{c^2 - 1}{1 + c^2}\right) \equiv \varphi_h,$$

and the range of arccos is $[0, \pi)$. In the present example, because of no flow induced and asymmetry of the data in the boundary conditions, some singularity sources cancel out one another for the first few moments. Hence, we here focus on the x-component of the heat flow $p_0(2\mathcal{R}T_0)^{1/2}Q_x$ on the positive z-axis at $z = s$ ($p_0 = \rho_0\mathcal{R}T_0$ is the reference pressure), which is free from such cancellations:

$$Q_x(z = s) = \int \zeta_x(\zeta^2 - \frac{5}{2})\phi E d\boldsymbol{\zeta} = Q_\mathrm{v} + Q_\mathrm{c},$$
$$Q_\mathrm{v}/\beta = -4\pi^{-3/2}\int_0^{\varphi_*} d\varphi_\zeta \cos^2\varphi_\zeta\Big(\int_0^{\theta_t} d\theta_\zeta \sin^2\theta_\zeta r_w + \int_{\theta_t}^{\pi} d\theta_\zeta \sin^2\theta_\zeta\Big)$$
$$- 4\pi^{-3/2}\int_{\varphi_*}^{\varphi_h} d\varphi_\zeta \cos^2\varphi_\zeta\Big(\int_0^{\theta_e} d\theta_\zeta \sin^2\theta_\zeta r_w + \int_{\theta_e}^{\pi} d\theta_\zeta \sin^2\theta_\zeta\Big),$$
$$Q_\mathrm{c}/\beta = -2\pi^{-3/2}\int_{\varphi_h}^{\pi-\varphi_h} d\varphi_\zeta \cos^2\varphi_\zeta\Big(\int_0^{\theta_e} d\theta_\zeta \sin^2\theta_\zeta r_w + \int_{\theta_e}^{\pi} d\theta_\zeta \sin^2\theta_\zeta\Big).$$

Here Q_v is the contribution from the range of azimuth angle corresponding to the convex part of the inner boundary, Q_c is that from the range of azimuth angle corresponding to the concave part of the inner boundary. They are plotted together with Q_x in Fig. 9(a). As is clear from Fig. 9(a), the double-log plots for Q_x and Q_v become straight lines with slope $1/2$ for small s, which means that Q_x and Q_v change from their values on the boundary in proportion to $s^{1/2}$ near the boundary. The semi-log plot for Q_c in Fig. 9(a) becomes straight line with non-zero slope for small s, which means that Q_c changes from its

value on the boundary in proportion to $s \ln s$ near the boundary. Therefore, among the two types of singularity sources, the contribution from the convex part is dominant, as expected. In order to estimate the magnitude of the singularity sources from the numerical data, we obtained as well the coefficient $c_{\rm s}$ of the fitting curve $c_{\rm s} s^{1/2}$ to $|Q_x(s) - Q_x(0)|/\beta$ determined by the least squares fitting with five sampling points within the distance 1.3×10^{-6} from the boundary. The coefficients c_ℓ and $c_{\rm r}$ of the fitting curve $-c_\ell s \ln s + c_{\rm r} s$ to $|Q_{\rm c}(s) - Q_{\rm c}(0)|/\beta$ were also obtained in the same way. The results are plotted with markers in Fig. 9(b), together with the fraction of the convex part in azimuth angle (the dashed line). As is clear from Fig. 9(b), the fraction of the convex part decreases with increasing c; the $s^{1/2}$-dependence of Q_x is weaken accordingly. The $s \ln s$-dependence of $Q_{\rm c}$ grows, on the contrary, in accordance with the growth of fraction of the concave part, when c increases up to around 10^2. These are consistent with our prediction in (Case 2) in Sect. 3. Incidentally, if c increases further and beyond around 10^2, the $s \ln s$-dependence of $Q_{\rm c}$ becomes weaker [see the most right two closed circles in Fig. 9(b)]. This is due to the present setting of surface temperature distribution. In the present setting, as c grows largely, the variation of temperature along the surface becomes milder with the fraction of the concave part almost unchanged, and $s \ln s$-dependence turns to decrease accordingly [see (9) with $\nu = 0$ in Sect. 2.1.3].

5 Concluding remarks

We have discussed in detail the blow up of gradients of macroscopic quantities in approaching the boundary in steady rarefied gas flows, with the aid of partial and quasi-full models of the linearized Boltzmann equation. The source term in the quasi-full model mimics the essential spatial property of $\mathcal{K}[\phi]$ and thus our discussion applies to the original linearized Boltzmann equation as well. As to the nonlinear Boltzmann equation, we are lacking evidence for the spatial property of the nonlinear collision term near the boundary. If the nonlinear collision term spatially behaves as the linearized one does, our statements should apply, as they are, to the nonlinear Boltzmann equation as well. Incidentally, the nonlinearity of the boundary data does not affect our discussions on the collisionless gases, some examples of which can be found in [14].

As briefly mentioned in the introduction, our results also give the insight on the difference in structure between the S layer and the Knudsen layer at their bottoms. According to [12], the S layer is the region where the discontinuity of VDF remains around a convex body, while the Knudsen-layer is the kinetic boundary layer which has been formulated as a half-space problem (the so-called Milne and/or Kramers problems) based on the planar approximation to the boundary geometry in the stretched scale of spatial coordinates. Indeed, the structure of the S layer around a circular cylinder in [6] shows the square-root growing rate in the normal distance from the cylinder surface,

which agrees with our theoretical conclusions. The same growing rate can be found in the problem of the thermophoresis around a spherical particle [11], though the explicit form is not given in [11] (see the Acknowledgements). The growing rate in these observations is in marked contrast with the structure of the Knudsen-layer at its bottom. Indeed, the data of the Knudsen-layer corrections tabulated in, e.g., [10, Table 3.3] and [9, Table 3.3] for the BGK model, [5, Table 5.2] for the hard sphere molecules, show logarithmic type ($s \ln s$) dependence on the normal distance s, which agrees with our results for the planar boundary case.

Recently, there are several attempts in the literature to extend a classical approach such as the Navier-Stokes equation with adjustable viscosity, aiming at the full description of the kinetic boundary layer in the slip-flow regime. The presence of the kinetic effect discussed here shows a limitation of such an approach.

Acknowledgements

We thank Yutaro Akahoshi and Katsuyuki Inui for their helps in double checking the numerical data in Sect. 4.3. The research note of Kazuo Aoki of Ref. [11] was helpful in assessing our insight on the internal structure of the S layer. We really appreciate his courtesy.

References

1. Bhatnagar, P.L., Gross, E.P., Krook, M.: A model for collision processes in gases. I. Small amplitude processes in charged and neutral one-component systems. Phys. Rev. **94**, 511–525 (1954)
2. Chen, I.K.: Boundary singularity of moments for the linearized Boltzmann equation. J. Stat. Phys. **153**, 93–118 (2013)
3. Guo, Y., Kim, C., Tonon, D., Trescases, A.: BV-regularity of the Boltzmann equation in non-convex domains. Arch. Rat. Mech. Anal. **220**, 1045–1093 (2016). DOI 10.1007/s00205-015-0948-9
4. Guo, Y., Kim, C., Tonon, D., Trescases, A.: Regularity of the Boltzmann equation in convex domains. Inv. Math. **207**, 115–290 (2016). DOI 10.1007/s00222-016-0670-8
5. Hattori, M., Takata, S.: Second-order Knudsen-layer alanysis for the generalized slip-flow theory I. Bul. Inst. Math. Academia Sinica (New Series) **10**, 423–448 (2015)
6. Sone, Y.: New kind of boundary layer over a convex solid boundary in a rarefied gas. Phys. Fluids **16**, 1422–1424 (1973)
7. Sone, Y.: Highly rarefied gas around a group of bodies with various temperature distributions I. small tempearature variation. J. Méc. Théor. Appl. **3**, 315–328 (1984)
8. Sone, Y.: Highly rarefied gas around a group of bodies with various temperature distributions II. arbitrary temperature variation. J. Méc. Théor. Appl. **4**, 1–14 (1985)
9. Sone, Y.: Kinetic Theory and Fluid Dynamics. Birkhäuser (2002)
10. Sone, Y.: Molecular Gas Dynamics. Birkhäuser (2007). URL http://hdl.handle.net/2433/66098
11. Sone, Y., Aoki, K.: Negative thermophoresis: Thermal stress slip flow around a spherical particle in a rarefied gas. In: S.S. Fisher (ed.) Rarefied Gas Dynamics, pp. 489–503. AIAA (1981)
12. Sone, Y., Takata, S.: Discontinuity of the velocity distribution function in a rarefied gas around a convex body and the S layer at the bottom of the Knudsen layer. Transp. Theor. Stat. Phys. **21**, 501–530 (1992)

13. Takata, S., Funagane, H.: Singular behaviour of a rarefied gas on a planar boundary. J. Fluid Mech. **717**, 30–47 (2013)
14. Takata, S., Yoshida, T., Noguchi, T., Taguchi, S.: Singular behavior of the macroscopic quantities in the free molecular gas. Phys. Fluids **28**, 022,002–1–15 (2016)
15. Welander, P.: On the temperature jump in a rarefied gas. Ark. Fys. **7**, 507–553 (1954)